Modified covariance beamformer for solving MEG inverse problem in the environment with correlated sources

Aleksandra Kuznetsova, Yulia Nurislamova, Alexei Ossadtchi*

Center for Bioelectric Interfaces, Higher School of Economics, Moscow 101000, Russia

A B S T R A C T

Magnetoencephalography (MEG) is a neuroimaging method ideally suited for non-invasive studies of brain dynamics. MEG's spatial resolution critically depends on the approach used to solve the ill-posed inverse problem in order to transform sensor signals into cortical activation maps. Over recent years non-globally optimized solutions based on the use of adaptive beamformers (BF) gained popularity.

When operating in the environment with a small number of uncorrelated sources the BFs perform optimally and yield high spatial resolution. However, the BFs are known to fail when dealing with correlated sources acting like poorly tuned spatial filters with low signal-to-noise ratio (SNR) of the output timeseries and often meaningless cortical maps of power distribution.

This fact poses a serious limitation on the broader use of this promising technique especially since fundamental mechanisms of brain functioning, its inherent symmetry and task-based experimental paradigms result into a great deal of correlation in the activity of cortical sources. To cope with this problem, we developed a novel data covariance modification approach that allows for building beamformers that maintain high spatial resolution when operating in the environments with correlated sources.

At the core of our method is a projection operation applied to the vectorized sensor-space covariance matrix. This projection does not remove the activity of the correlated sources from the sensor-space covariance matrix but rather selectively handles their contributions to the covariance matrix and creates a sufficiently accurate approximation of an ideal data covariance that could hypothetically be observed should these sources be uncorrelated. Since the projection operation is *reciprocal* to the PSIICOS method developed by us earlier (Ossadtchi et al., 2018) we refer to the family of algorithms presented here as ReciPSIICOS.

We assess the performance of the novel approach using realistically simulated MEG data and show its superior performance in comparison to the classical BF approaches and well established MNE as a method immune to source synchrony by design. We have also applied our approach to the MEG datasets from the two experiments involving two different auditory tasks.

The analysis of experimental MEG datasets showed that beamformers from ReciPSIICOS family, but not the classical BF, discovered the expected bilateral focal sources in the primary auditory cortex and detected motor cortex activity associated with the audio-motor task. In most cases MNE managed well but as expected produced more spatially diffuse source distributions. Notably, ReciPSIICOS beamformers yielded cortical activity estimates with SNR several times higher than that obtained with the classical BF, which may indirectly indicate the severeness of the signal cancellation problem when applying classical beamformers to MEG signals generated by synchronous sources.

1. Introduction

Magnetoencephalography (MEG) is a noninvasive neuroimaging method hallmarked by the millisecond scale temporal resolution and subcentimeter spatial resolution. As such, this method is very well suited for studying the fine features of spatio-temporal dynamics exhibited by neural circuits. The high temporal resolution of MEG is concomitant to the nature of the underlying electrophysiological processes in the brain tissue. As to the spatial resolution, it crucially depends on how the ill-posed inverse problem is approached to recover the distribution of neu-

ral sources from the magnetic field measurements around the head. Because the MEG inverse problem is inherently ill-posed no universal approach for solving it exists and each method makes specific assumptions about the properties of the neuronal activity.

One assumption common in the MEG literature is that the neuronal substrate that produces the observed data can be approximated by a small number of active focal sources typically represented by a set of equivalent current dipoles (Hamalainen and Hari, 1993). This multiple equivalent current dipoles (ECD) model originally implied the use of the least squares dipole fit to identify the location and orientation parameters of the dipoles (An et al., 2008). In practice the parametric ECD model can be used to represent spatially extended sources which was demonstrated in De Munck et al. (1988) where dipole model error was studied for extended sources of the simulated visual evoked potentials (VEPs). The difficulties associated with this approach are the unknown number of sources and the need to solve a non-convex optimization task can be gracefully resolved with Multiple Signals Classification (MUSIC) family of methods, e.g. RAP-MUSIC (Mosher and Leahy, 1999). This method allows constructing a constellation of ECDs explaining the observed data produced by several simultaneously active (but not synchronous) sources. Recent extension called tRAP-MUSIC (Mäkelä et al., 2018) furnishes an elegant approach that yields an improved estimate on the number of true active sources present in the data. An additional attractive feature of MUSIC family of approaches is that they do not invert data covariance matrix which avoids the need to employ regularization strategies that may bias the results. However, MUSIC methods can only find source location and are not designed for the source timeseries estimation task. Although the absence of data covariance inversion step make MUSIC approaches fairly robust against source timeseries correlations, applying MUSIC family methods to the data generated by synchronous sources (with source timeseries correlation close to 1) requires an explicit scan for synchronized cliques which may be time-consuming and impractical, especially when such cliques comprise more than two sources.

More than two decades ago local linear estimators were introduced as an alternative approach to estimating source distributions and timeseries of specific neuronal sources from MEG and EEG data (Van Veen et al., 1997). This technique is based on the adaptive beamforming principle (Borgiotti and Kaplan, 1979) originally developed to detect sources in radar signals. In neuroimaging we employ adaptive linearly constrained minimum variance (LCMV) beamformers (Greenblatt et al., 2005; Sekihara et al., 2001; Van Veen et al., 1997) both in the scanning mode and for estimation of neuronal source timeseries. To recover activity of a given source the LCMV beamformer finds a spatial filter by solving the optimization task to minimize the output power under the constraint of unit gain in the "direction" of the given source. Spatial distributions delivered by beamformers when operated in optimal conditions tend to be focal, which represents the "most interesting feature" of this approach as described in Borgiotti and Kaplan (1979). However, as a result of the "greedy" optimization linear dependencies between the neuronal source timeseries are utilised by the algorithm to minimize the output power (Sekihara and Nagarajan, 2008). This undesired phenomenon is called signal cancellation. Therefore applying the original LCMV beamforming approach we must assume that the measurements are generated by sources with uncorrelated timeseries.

In reality, in the neuroimaging applications this assumption is often violated which leads to suboptimal performance of the adaptive beamformers. Thus, cortical sources exhibit transient synchrony (Varela et al., 2001) that manifests ongoing integrative processes (Fries, 2015). Another reason for such synchronization is the time-locking of brain activity (called event-related potentials, ERPs) to task events, such as movement or stimulus onset, for a wide range of cognitive, motor and sensory paradigms (Gascoyne et al., 2016). Synchronous ERPs often occur in both hemispheres at the functionally homologous areas. Bidirectional interaction of neuronal populations also leads to synchronization of their activity.

In this paper we propose a model-based extension of the LCMV beamforming that makes it robust against source synchrony and allows for reliable estimation of both locations and timeseries of synchronous sources. To explain the basic concept of this paper, we first illustrate the two opposite but related problems of (1) Estimating functional connectivity based on the indirect measurements and (2) Estimating source timeseries or source power distribution using adaptive beamforming. The problem of the former is the presence of artifacts of volume conduction: truly independent sources result into correlated sensor activity. The goal is to tune away from the volume conduction and estimate true source correlations. However, the presence of a non-trivial solution to the first problem, i.e. the presence of sources with true dependencies, is the problem of the latter: correlated sources lead to well known and unwanted signal cancellations in adaptive beamforming. As already stated, the original adaptive beamformer is optimal if all source activities are uncorrelated, i.e. a situation where any observed functional connectivity (measured as correlation) is purely an artifact of volume conduction. Correlated sources cause a significant reduction in the SNR when adaptive beamformers are used to process the data (Sekihara and Nagarajan, 2008).

Here we focus on the latter problem and develop an improvement for adaptive beamforming to make it robust against source correlations. The key component of an adaptive beamformer is the data covariance matrix that contains information about both the source-power distribution and about the linear source dependencies. The manifestation of linear dependencies present in the data covariance matrix is implicitly used by the LCMV beamformer optimal weights expression to further minimize beamformer output variance. Here we propose a procedure that uses data covariance generative model to selectively handle covariance matrix components to create a close approximation of an ideal data covariance matrix that would hypothetically be observed in the absence of correlation between source timeseries. Importantly, our covariance modification procedure is data-independent. It relies only on the forward model and can be considered as a deterministic extra step in building an adaptive LCMV-based inverse operator.

This paper is organized as follows. First we introduce the data model and describe the original adaptive beamforming approach (Van Veen et al., 1997). We then briefly illustrate both analytically and graphically the problem of correlated sources and emphasize the situation when more than two coupled sources are present. Next, having introduced the basic concepts and outlined the problem of correlated source timeseries we review the existing solutions and stress that most of them focus on the idea of nulling the sources identified as coupled to the target one. This approach may become impractical when the number of coupled sources is large and therefore next we introduce two covariance modification methods that allow us to suppress the manifestation of source correlations in the data covariance matrix without the need to identify the synchronized cliques. Using extensive simulations and real data from two paradigms we compare the performance of the adaptive beamformers built using the original and the modified data covariance matrices. We also match the performance of the beamforming approaches against the minimum-norm estimation technique (Hämäläinen and Ilmoniemi, 1994) that is (1) by design not affected by source timeseries correlation and (2) represents a solid and trusted reference that was also shown to manage well with localizing focal source in real data (Komssi et al., 2004). In the discussion we summarize our findings and outline the shortcomings and potential directions to further advance the proposed approach.

2. Methods

2.1. Data model

We assume that event-related potentials (ERPs) measured with electrophysiological methods such as electroencephalography (EEG) and magnetoencephalography (MEG) can be represented as a superposition

of the contributions from a finite number of sources. Only the contributions that are sufficiently phase-locked to the task onset moment make it through the averaging procedure and form the evoked response (Luck and Kappenman, 2011). The observation equation linking vector $\mathbf{s}(t)$ of the averaged source-space activity with ERP's timeslice $\mathbf{x}(t)$ measured by the array of M sensors at time instance t can be written as

$$\mathbf{x}(t) = \sum_{i=1}^{R} \mathbf{g}_i s_i(t) + \mathbf{n}(t) = \mathbf{Gs}(t) + \mathbf{n}(t). \tag{1}$$

where $\mathbf{x}(t)$ is $[M \times 1]$ vector and $\mathbf{s}(t) = \left[s_1(t), \ldots, s_R(t) \right]^T$ is an $[R \times 1]$ vector, as we assume, that this evoked activity is generated by a relatively small number R of focal cortical sources. Here $\mathbf{g}_i$ is the topography of the i-th equivalent current dipole and $\mathbf{G} = \left[\mathbf{g}_1, \ldots, \mathbf{g}_R \right]$ is a matrix of the oriented source topographies. Noise term $\mathbf{n}(t)$ represents the sum of the remainders of the induced and task unrelated activity that is supposed to be sufficiently suppressed by the event-related averaging procedure. For compactness in the presentation that follows we will stick to the fixed orientation source model. However, in Section 2.5 we show how to handle the unknown source orientations and apply the proposed methodology to the vector beamformer (Sekihara et al., 2001).

One of the key assumptions implicit in this ERP data model is that the stimulus-locked cortical activation profiles are expected to be focal. The number of active stimulus-related sources R is usually unknown, but it is assumed to be several orders of magnitude less than the total number of cortical sources. Note that in this paper we suggest an improvement of the standard beamformer without making additional assumptions about the spatial distribution of the sources as compared to beamformers themselves. Thus (1) represents basically the same source model as the one in (Van Veen et al., 1997).

It is customary to consider the MEG data in the space of virtual sensors obtained by calculating the projection coefficients onto a subset of principal directions of the forward model matrix. The formulation presented here accommodates this point of view without any conceptual changes. The value of M corresponding to the number of physical sensors will then reflect the number of virtual sensors corresponding to the number of principal directions capturing a specific percentage of variance in the original forward model. Correspondingly, the forward matrix $\mathbf{G}$ will be replaced by the product with the matrix containing the coordinates of principal components in the original space.

The LCMV beamforming approach extended here does not formally require the spatial whiteness of the additive noise term (Van Veen et al., 1997) and therefore we do not make assumptions regarding its spatial covariance structure. Whole data covariance is assumed to have full rank.

The active source locations are unknown, and finding them is the goal of the EEG and MEG inverse problem solving. We approach this problem with the knowledge of the forward model that matches every i-th location of the dipolar sources with a topography vector $\mathbf{g}_i$ that contains the weights for the contribution of the i-th unit dipole to the sensor measurements. Our goal is then to identify the grid nodes containing active dipoles. Sufficient accuracy of computing $\mathbf{g}_i$ is a strong requirement to ensure adequate performance of the inverse solvers, including adaptive beamformers.

2.2. Adaptive LCMV beamformer

Adaptive linearly constrained minimum variance (LCMV) beamformer (Sekihara et al., 2001; Van Veen et al., 1997) is a local linear estimator with a unit gain weight constraint (Greenblatt et al., 2005). Over the recent years, this approach gained popularity as an efficient inverse solver of the MEG inverse problem (Darvas et al., 2004).

Due to the fundamental limitations of the electromagnetic inverse problem, it is impossible to globally suppress contribution from all non-target sources. Therefore, within the beamforming approach, the problem of finding the spatial filter weights is formulated locally as mini-

mizing the spatial filter output variance under the unit gain constraint with respect to the source of interest.

Beamformers can be used to estimate the activity of a specific ROI or in a scanning mode to assess the distribution of activity over the entire cortex. Various forms of beamformers exist that can be classified based on the source-space and sensor-space norms (Greenblatt et al., 2005). Unlike global estimators (MNE, wMNE, MCE, etc.), beamformers tuned to different cortical locations do not depend on each other and their summed output projected back to the source space is generally not supposed to be equal to the measured data $\mathbf{X}$.

Good spatial resolving power is one of the most attractive features of the adaptive beamforming technique (Borgiotti and Kaplan, 1979). It is achieved using the data covariance matrix that conveys the information about the subset of active sources to the beamformer. This information is then used by the beamformers to efficiently distribute the available degrees of freedom to suppress only these active sources.

2.2.1. Adaptive beamforming principle

Consider an elementary cortical dipolar source with free orientation at $\mathbf{r}_i = [x_i, y_i, z_i]$. To reconstruct activity via vector LCMV beamformer from the EEG or MEG data, one uses a spatial filter $\mathbf{b}_i$ tuned to this dipolar source. These weights are calculated as the solution to the following optimization problem (Sekihara et al., 2001)

$$\begin{aligned} \underset{\mathbf{b}_i}{\text{minimize}} \quad & \mathbf{b}_i^T \mathbf{C}_x \mathbf{b}_i \\ \text{subject to} \quad & \mathbf{b}_i^T \mathbf{g}_i = 1, \end{aligned} \tag{2}$$

where $(\cdot)^T$ is the transpose operator, $\mathbf{C}_x = E\{\mathbf{x}(t)\mathbf{x}(t)^T\}$ is the sensor-space covariance matrix, matrix $\mathbf{g}_i = \mathbf{g}(\mathbf{r}_i)$ is a topography of the i-th source. Using Lagrange multipliers method, it can be shown that the optimal solution is

$$\mathbf{b}_i^T = [\mathbf{g}_i^T \mathbf{C}_x^{-1} \mathbf{g}_i]^{-1} \mathbf{g}_i^T \mathbf{C}_x^{-1} \tag{3}$$

The calculated spatial filters $\mathbf{b}_i$ could then be used to reconstruct the source timeseries vector estimates as

$$\widehat{\mathbf{s}}_i(t) = \mathbf{b}_i^T \mathbf{x}(t). \tag{4}$$

It is also possible to employ the beamformer in the scanning mode and compute power distribution profile $\sigma_i^2 = \text{Var}(\mathbf{r}_i)$ for the entire set of N cortical locations $\mathbf{r}_i$, $i = 1, \ldots, N$ which can be done without the explicit computation of $\mathbf{b}_i$ (Sekihara and Nagarajan, 2008):

$$\sigma_i^2 = \mathbf{b}_i^T \mathbf{C}_x \mathbf{b}_i = [\mathbf{g}_i^T \mathbf{C}_x^{-1} \mathbf{g}_i]^{-1}. \tag{5}$$

As follows from Eqs. (3) and (5), given the forward model, the covariance matrix fully determines the beamformer weights and the output power of source estimates when applied to the data $\mathbf{x}(t)$.

The described approach does not introduce any assumptions on the number of active sources or their spatial distribution. However, the LCMV adaptive beamformer assumes that the measured neural activity is produced by a small number of focal cortical sources (Borgiotti and Kaplan, 1979).

2.2.2. Adaptive beamforming in the environment with correlated sources

Despite the high localization efficiency and high spatial resolution, adaptive LCMV beamformers suffer from the signal cancellation problem when operating in the suboptimal environment. The optimal spatial filters calculated in (3) reflect activity of intrinsic sources correctly only when the measurements are generated by a small number of focal sources with uncorrelated timeseries.

These assumptions, however, are rarely met in the real experimental conditions because the brain integrative mechanisms result in a high level of synchrony across different areas (Fries, 2015). Thus, synchronous, stimulus-locked responses occur in many cortical areas, such as, for instance, ERPs occurring in bilateral, functionally homologous locations (Gascoyne et al., 2016).

Such correlation of sources causes significant reduction in the SNR of sources timeseries estimated with adaptive beamformers. For example,
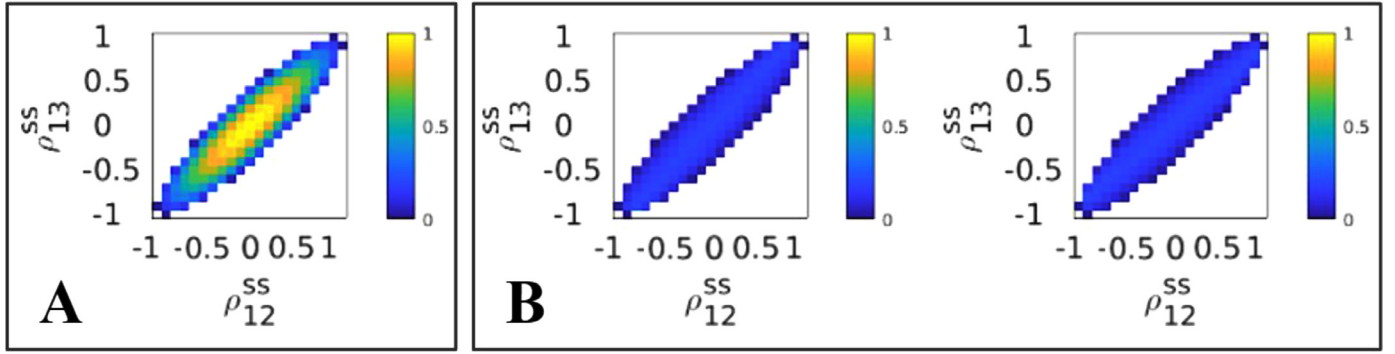
Fig. 1. LCMV beamformer reconstruction in the case of three active sources with pairwise correlations ρ_{12}^{ss}, ρ_{13}^{ss} and $\rho_{23}^{ss} = 0.9$. The estimated variance $\hat{\sigma}_i$, $i = 1, 2, 3$ for each of the three sources as a function of pairwise correlation ρ_{12}^{ss}, ρ_{13}^{ss} is color-coded into the heat-maps. In each plot, the axis reflect coupling of the first source, $\mathbf{r}_1$ to the other two sources $\mathbf{r}_2$ and $\mathbf{r}_3$ quantified by the correlation coefficients ρ_{12}^{ss} and ρ_{13}^{ss}. The impossible combinations of correlation coefficient values given unit variance sources are shown in white.

it can be shown (Sekihara and Nagarajan, 2008), that in the case of two interacting sources the estimated power of each source decreases as a quadratic function of the correlation coefficient of their timeseries and in the case of unit source variance, the output power can be expressed as

$$\hat{\sigma}_i^2 = 1 - (\rho_{12}^{ss})^2, \quad i = 1, 2 \qquad (6)$$

As follows from (6) in the case of complete synchrony, the adaptive beamformer will simply output zero. Intuitively this can be understood as follows. In order to meet the constraint, the beamformer provides unit gain for the target source. The functional optimized by the adaptive beamformer requires minimization of the output power. In the presence of another source with correlated activity, the beamformer adjusts the weight vector in such a way that, on the one hand, the gain of unity constraint is met, and on the other hand, the activity of the correlated sources is subtracted from the target activity to minimize the output power. Therefore, in the case of perfect correlation, the beamformer produces a zero SNR with respect to the activity of the target source.

The situation is aggravated in the environment with larger number of correlated source. Even moderate correlation of source timeseries causes significant reduction in the SNR of adaptive beamformer based estimates. Consider an environment with three active unit variance sources $\mathbf{r}_1, \mathbf{r}_2, \mathbf{r}_3$ with activation timeseries characterized by pairwise correlation coefficients $\rho_{12}^{ss}, \rho_{13}^{ss}, \rho_{23}^{ss}$.

It is relatively straightforward to show, that in this case the adaptive LCMV estimated source power $\hat{\sigma}_i$, $i = 1, 2, 3$ depends on the pairwise correlation coefficients ρ_{ij}^{ss} as

$$\hat{\sigma}_1^2 \propto \frac{F}{(\rho_{23}^{ss})^2 - 1}, \quad \hat{\sigma}_2^2 \propto \frac{F}{(\rho_{13}^{ss})^2 - 1}, \quad \hat{\sigma}_3^2 \propto \frac{F}{(\rho_{12}^{ss})^2 - 1}, \qquad (7)$$

where

where $F = \left(\rho_{12}^{ss}\right)^2 + \left(\rho_{13}^{ss}\right)^2 + \left(\rho_{23}^{ss}\right)^2 - 2\rho_{12}^{ss}\rho_{13}^{ss}\rho_{23}^{ss} - 1$.

Panels A and B of Figure 1 show color-coded estimated power of the three sources $\mathbf{r}_1$, $\mathbf{r}_2$ and $\mathbf{r}_3$ for various degrees of coupling between the first source and the other two sources when $\mathbf{r}_2$ and $\mathbf{r}_3$ are strongly coupled, $\rho_{23} = 0.9$. As expected, the output power of the second and the third sources is reduced primarily due to their strong mutual coupling, Fig. 1.B. In this case low SNR in the estimates of $\mathbf{r}_2$ and $\mathbf{r}_3$ complicates their detection and makes it problematic to implement the strategies suggested in Dalal et al. (2006); Popescu et al. (2008) to ameliorate the problems caused by source correlation. Additionally, we also observe a rapid reduction in the estimate of $\mathbf{r}_1$ power with the growth of coupling between this first source and either of the two remaining sources, Fig. 1.A.

In real life setting this situation may occur, for example, in an auditory-motor experimental paradigm, where the subject is required to

perform a motor action (e.g. press the button) in response to a deviant auditory stimulus. According to our indexing scheme source $\mathbf{r}_1$ models sensory-motor response and sources $\mathbf{r}_2$ and $\mathbf{r}_3$ are located bilaterally in the primary auditory cortex and respond synchronously to the auditory stimulus.

Another likely scenario is when the source distribution is represented in the form of two groups of sources with significant synchrony within each such group but no correlation between the groups. In this case the within group synchrony will affect beamformer's performance and will result in timeseries with underestimated amplitudes and erroneous source distributions.

2.2.3. Existing solutions

Several approaches have been developed to improve beamforming in the presence of correlated sources. (Dalal et al., 2006) suggested that the entire region that may potentially include a source correlated to the activity in the region of interest (ROI) should be suppressed. This idea can be implemented using an SVD derived constraint based on the topography of the cortical patch containing the interfering source. This approach requires an *apriori* knowledge of the locations of correlated sources. Nulling the activity of multiple regions (or spatially-extended ones) with this method reduces the number of degrees of freedom, that otherwise could be used for suppressing the interfering sources.

Brookes et al. (2007) suggested building a beamformer based on the constraints that are calculated from the topographies of correlated sources using their linear combination. An "amplitude optimization" routine was suggested to compute the optimal mixing coefficients for this procedure. Application of this method to real data requires explicit scanning over all possible pairs using a coarse grid, which is not time efficient and prone to errors if the seed source is set *apriori*.

Two beamformers that allow to overcome correlated sources issue were evaluated in Popescu et al. (2008): (1) a linearly constrained minimum variance beamformer with partial sensor coverage (LCMV-PSC), and (2) a multiple constrained minimum-variance beamformer with coherent source region suppression (MCMV-CSRS). It was demonstrated that the latter exhibits precise localization and minimal amplitude and phase distortion for a broad range of relative positions of the interfering source within the suppression region. With this method, again, degrees of freedom are consumed because of the assumption regarding the location of the interfering source that maintains the regional zero constraint.

Quraan and Cheyne (2010) compared various solutions available to the date of that publication to cope with correlated sources in beamforming. When prior information about the location of correlated sources is available, the method of beamforming with coherent source region suppression described in Dalal et al. (2006) appeared to be the most effective, including the case of closely located (3 cm apart) correlated sources. The authors concluded that this solution, when carefully exer-

cised, can significantly improve localization accuracy, but does not fully solve the amplitude bias problem.

Diwakar et al. (2011) introduced a dual-core beamforming idea, which is an extension of Sekihara's vectorized LCMV approach (Sekihara et al., 2001). Dual-core beamformer is built using the constraint created from the topographies of two spatially disjoint regions. This approach allows for finding the pairs of highly correlated sources and eliminates the computationally expensive search for topographies mixing parameter and optimal dipole orientation required in the approach of Brookes et al. (2007).

The approaches based on finding pairs of correlated sources would, for example, fail to detect a hub coupled simultaneously to more than one additional source. Further, as our simulations show, synchrony between more than two sources has a complex effect on the suppression of the beamformer output power. Therefore, in a number of practical situations, the beamformers limited to considering only a pair of sources could fail. Moiseev et al. (2011) presented a detailed treatment of the multiple constrained minimum-variance beamformers with coherent source region suppression (MCMV-CSRS) and offered a set of practical solutions and scanning statistics to be used for identifying cortical regions with correlated activity.

The approaches for coping with source synchrony problem that we have described so far are conceptually similar and spin around the idea of suppressing the activity of the sources correlated to the current ROI. Additional insights into the problem of adaptive beamfoming in the environment with correlated sources could be gained from the data covariance matrix, which contains the information about source synchrony. Formulation of the minimum variance adaptive beamforming optimization problem implies the absence of correlation of the underlying sources which leads to a specific structure of the data covariance matrix. When this structure is violated the adaptive beamforming algorithm results in significant suppression of the SNR of the estimated source timeseries, and in the case of perfect synchrony the adaptive beamformer would completely cancel the signal.

The approach we propose here is based on the analysis of the structure of the data covariance matrix. Kimura et al. (2007) previously developed a method that is conceptually close to ours. They used a forward model and the least squares approximation approach to find an estimate of the source-space covariance matrix that corresponded to the interaction of a small number of sources. They then nulled the off-diagonal elements of this matrix and projected it back to the sensor space. This new decorrelated matrix was used for building the conventional beamformers. The performance of this approach depends on the estimated number of active sources chosen to comprise the source-space covariance matrix. The selection of the number of sources to be represented in the source-space covariance matrix is a non-trivial problem that affects the performance of this technique.

Here we propose an alternative way to modify data covariance matrix that makes adaptive LCMV beamforming robust against correlation of neural sources activity but does not require the full blown source modelling. In contrast to the approach described in Kimura et al. (2007), our covariance modification procedure does depend on the data. The proposed covariance modification procedure creates a close approximation of an ideal data covariance that could hypothetically be observed in the absence of correlation of source timeseries. It relies only on the whole head forward model and can be considered as a deterministic extra step in building an adaptive LCMV-based inverse operator.

In our approach, we consider the sensor-space data covariance matrix $\mathbf{C}_x$ as an element of M^2-dimensional vector space and derive its expression as a function of active source topographies scaled by intrinsic source timeseries variance and covariance values. We then employ a data independent projection procedure to mitigate the contribution explained by coupling of intrinsic sources. This way the modified covariance matrix $\widetilde{\mathbf{C}}_x$ approximates the one that could have been obtained should the same but non-interacting constellation of sources is mea-

sured. We then apply the standard beamforming approach but use this modified data covariance matrix to compute the beamformer weights.

2.3. ReciPSIICOS beamforming

In this section we introduce the new beamformer modification, which is immune to the contributions from correlated sources in the data. The key component of the proposed algorithm is the projection procedure complementary to the PSIICOS (Ossadtchi et al., 2018) introduced by us earlier.

We originally designed PSIICOS projection technique for connectivity analysis, particularly for non-invasive detection of true zero-phase interactions between sources which addressed problem (1) Estimating functional connectivity outlined in the introduction. The procedure employs a projection operation applied to the sensor space cross-spectral matrix treated as an element of M^2-dimensional vector space. We showed that PSIICOS could sufficiently well disentangle the subspace containing spatial leakage power from the subspace containing the contributions from the true zero-phase coupling of sources having different locations.

Here we address problem (2) Estimating source timeseries or source power distribution using adaptive beamforming and use a similar projection based approach for solving this complementary problem. Instead of suppressing the variance in the subspace filled with source power, we use the *complementary* version of PSIICOS projection to *emphasize* it and instead suppress the contributions to the *sensor* data covariance matrix the spatial components modulated by the *source*-space timeseries covariance. We refer to the new method as ReciPSIICOS because the proposed pipeline solves the problem reciprocal to that solved by PSIICOS.

2.3.1. General idea and vectorized sensor-space covariance matrix

$M \times M$ sensor-space covariance matrix $\mathbf{C}_x = E\{\mathbf{x}(t)\mathbf{x}^T(t)\}$ plays a pivotal role in adaptive beamforming. Vectorized covariance $vec(\mathbf{C}_x)$ of the evoked response can be expressed in terms of the elements c_{ij}^{ss}, $i, j = 1, ..., R$ of the source-space covariance matrix of R active sources and their topographies $\mathbf{g}_i$ as

$$vec(\mathbf{C}_x) = vec(E\{\mathbf{x}(t)\mathbf{x}^T(t)\}) = \sum_{i=1}^{R} vec(\mathbf{g}_i \mathbf{g}_i^T) c_{ii}^{ss}$$

$$+ \sum_{i=1}^{R} \sum_{j=i+1}^{R} vec(\mathbf{g}_i \mathbf{g}_j^T + \mathbf{g}_j \mathbf{g}_i^T) c_{ij}^{ss} + vec(\mathbf{C}_n) \quad (8)$$

where $\mathbf{C}_n$ is the noise covariance matrix.

Eq. (8) demonstrates that matrix $\mathbf{C}_x$ can be decomposed into two types of additive terms: auto-terms corresponding to the source power $\sum_{i=1}^{R} vec(\mathbf{g}_i \mathbf{g}_i^T) c_{ii}^{ss}$ and also the pairwise cross-products of source topographies weighted with source covariance coefficients $\sum_{i=1}^{R} \sum_{j=i+1}^{R} (\mathbf{g}_i \mathbf{g}_j^T + \mathbf{g}_j \mathbf{g}_i^T) c_{ij}^{ss}$. These cross-terms are present in the covariance matrix due to the non-zero off-diagonal elements c_{ij} of the source-space covariance matrix.

The very existence of the cross-terms in the source-space covariance matrix leads to the undesired performance of the adaptive beamformer. This happens because the weight vectors are formed in such a way that the correlated sources are utilized to minimize the beamformer output power.

To dwindle the contribution of source covariance terms to the sensor-space covariance matrix we propose to use a projector operating in the M^2-dimensional space. This processing pipeline is shown in Fig. 2. We apply this projector $\mathbf{P}$ to the vectorized data covariance matrix to weaken the contribution of the cross-terms. The resulting post-projection matrix when reshaped back approximates the sensor-space covariance that could have been obtained if no coupling was present. The obtained covariance matrix is then used in designing the LCMV beamformer according to the standard approach.

Next we propose two different approaches to building the $M^2 \times M^2$ projection matrix $\mathbf{P}$ dubbed ReciPSIICOS and whitened ReciPSIICOS.

1. Vectorize sensor-space covariance matrix

$$\mathbf{C}_x = \begin{bmatrix} c_{11} & c_{12} & \dots & c_{1M} \\ \vdots & \vdots & \vdots & \vdots \\ c_{M1} & c_{M2} & \dots & c_{MM} \end{bmatrix} \rightarrow \begin{bmatrix} c_{11} \\ c_{12} \\ \vdots \\ c_{1M} \\ \vdots \\ c_{MM} \end{bmatrix}$$

$$[M^2 \times 1]$$

$$\sum_{i=1}^{N}\sum_{j=i+1}^{N} vec(\mathbf{g}_i\mathbf{g}_j^T + \mathbf{g}_j\mathbf{g}_i^T)c_{ij}^{ss}$$

$$\sum_{i=1}^{N} vec(\mathbf{g}_i\mathbf{g}_i^T)c_{ii}^{ss}$$

2. Project and keep within PDM manifold

$$\widetilde{\mathbf{C}}_x = vec^{-1}\left(\begin{bmatrix} \tilde{c}_{11} \\ \tilde{c}_{12} \\ \vdots \\ \tilde{c}_{1M} \\ \vdots \\ \tilde{c}_{MM} \end{bmatrix}\right) = vec^{-1}\left(\mathbf{P} \cdot \begin{bmatrix} c_{11} \\ c_{12} \\ \vdots \\ c_{1M} \\ \vdots \\ c_{MM} \end{bmatrix}\right)$$

3. Apply usual beamformer with the projected matrix

$$\underset{\mathbf{b}_i}{\text{minimize}} \quad \mathbf{b}_i^T \widetilde{\mathbf{C}}_x^{abs} \mathbf{b}_i$$

$$\text{subject to} \quad \mathbf{b}_i^T \mathbf{g}_i = 1$$

Fig. 2. The main steps of the proposed approach. We manipulate with a the sensor-space covariance matrix $\mathbf{C}_x$ 1. We consider $\mathbf{C}_x$ as an element of a linear vector space and first vectorize it to enable standard operations defined in the linear vector spaces. The vectorized sensor-space covariance matrix $vec(\mathbf{C}_x)$ is shown with the red dot in the coordinate axes corresponding the trivial basis of the linear space of matrices. As a vector and based on the generative model (8) it can be viewed as a sum of two non-orthogonal vectors. The first vector is a linear contribution of sensor-space covariance auto-terms $\mathbf{g}_i\mathbf{g}_i^T$ modulated by source power $\sum_{i=1}^{R} vec(\mathbf{g}_i\mathbf{g}_i^T)c_{ii}^{ss}$. The second vector is a sum of the pairwise cross-products $\mathbf{g}_i\mathbf{g}_j^T$ of source topographies weighted with source space covariance coefficients $\sum_{i=1}^{R}\sum_{j=i+1}^{R}(\mathbf{g}_i\mathbf{g}_j^T + \mathbf{g}_j\mathbf{g}_i^T)c_{ij}^{ss}$. Our goal is to suppress the contribution of this second vector to $\mathbf{C}_x$ 2. We do this using the special precomputed projection matrix $\mathbf{P}$ that we apply to $vec(\mathbf{C}_x)$; the result is then reshaped back (vec^{-1}) into $M \times M$ matrix and care is taken to make sure $\widetilde{\mathbf{C}}_x^{abs}$ is a positive definite matrix. 3. Finally, adaptive beamformer spatial filters are calculated as usual but using the modified sensor-space data covariance.

2.3.2. ReciPSIICOS projection

The first approach to suppressing the manifestation of source activity correlation in the sensor-space covariance is based on projecting the vectorized data covariance $vec(\mathbf{C}_x)$ *onto* the source power subspace S_{pwr}^K defined here as the K-dimensional principal subspace of collection of the vectorized auto-products of source topographies $vec(\mathbf{g}_i\mathbf{g}_i^T)$, $i = [1, \dots, N]$, where N is the total number of sources in the forward model and K is the user defined parameter. See Fig. 2 and *Projection matrix* in Fig. 3. A rigorous criterion used to determine K is described in Section 2.4.

Importantly, unlike in Kimura et al. (2007) our approach for modification of the sensor-space covariance aimed at eliminating the manifestation of source activity correlation does not require estimating the the sources present in the data, neither their count nor locations. Rather, we use a projector matrix $\mathbf{P}$ informed by the sensor-space covariance generative model (8) and built using the forward model alone. To construct $\mathbf{P}$ we estimate the principal source power subspace S_{pwr}^K of some fixed dimension K capturing the largest proportion of variance that could have been potentially conveyed to the vectorized covariance matrix via $vec(\mathbf{g}_i\mathbf{g}_i^T)$, $i = [1, \dots, N]$ under the assumption of uniform distribution of activity across all N sources represented in the whole brain forward model matrix. This is exactly reciprocal to what is done in (Ossadtchi et al., 2018) where we solve the complementary problem of mitigating volume conduction effects and project the vectorized data

covariance *away* from the principal source power subspace S_{pwr}^K. The projection operator $\mathbf{P}$ obtained this way is directly complementary to that of PSIICOS.

More specifically, to build the projector we use the following sequence of steps:

1. Construct matrix $\mathbf{G}_{pwr}$, where columns correspond to the vectorized auto-products of topographies for all available N sources in the forward model. For compactness we are considering here the fixed orientation case and treat arbitrary source dipole orientations later in Section 2.5. We will denote the vectorized auto-product of topographies as $\mathbf{q}_{ii} = vec(\mathbf{g}_i\mathbf{g}_i^T) = \mathbf{g}_i \otimes \mathbf{g}_i^T$. Then, matrix $\mathbf{G}_{pwr}$ can be created by stacking $\mathbf{q}_{ii}$ as columns, i.e.

$$\mathbf{G}_{pwr} = [\mathbf{q}_{11}, \dots, \mathbf{q}_{ii}, \dots, \mathbf{q}_{NN}] \qquad (9)$$

2. Compute the singular value decomposition of matrix $\mathbf{G}_{pwr}$ obtained in the previous step, $\mathbf{G}_{pwr} = \mathbf{U}_{pwr}\mathbf{S}_{pwr}(\mathbf{V}_{pwr})^T$, and create the projector onto the principal source power subspace S_{pwr}^K

$$\mathbf{P} = \mathbf{U}_{pwr}^K\left(\mathbf{U}_{pwr}^K\right)^T, \qquad (10)$$

where $\mathbf{U}_{pwr}^K$ is formed from the first K left singular vectors. K is the projection rank and the only parameter which is needed to be chosen manually according to the guidelines given in Section 2.4. Note that this projection is complementary to that used
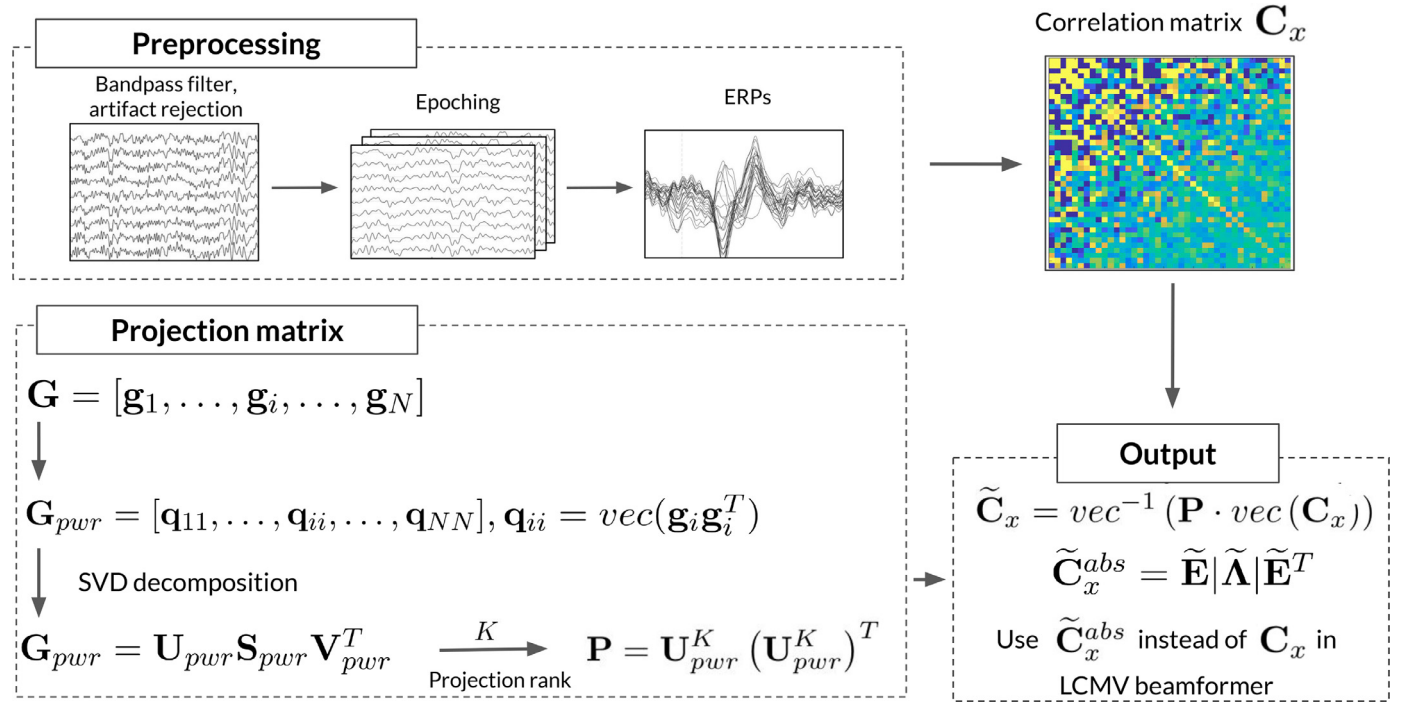
Fig. 3. A schematic presentation of the ReciPSIICOS algorithm. **Preprocessing:** We first epoch the data and compute evoked response fields. Usually, at this step to account for MEG data not being numerically full rank, we project the data into a space of virtual sensors derived from the forward model matrix and capturing user-specified percentage of its variance. **Projection matrix:** This is the main ingredient of our method. We are creating projection matrix **P** aimed at emphasizing the source power component (and at the same time suppressing source correlation component) of the sensor-space covariance, see Fig. 2 and expression (8) (green box). We operate in the product space of outer product of source topographies and collect all auto outer products $\mathbf{q}_{ii} = \mathbf{g}_i\mathbf{g}_i^T$, $i = 1, \ldots, N$ into a single matrix $\mathbf{G}_{pwr}$, see Eq. (13). Next, we perform SVD of this matrix to identify the subspace capturing the largest proportion of variance for any given dimension K. Then, using the first K left singular vectors $\mathbf{u}_pwr^1, \ldots, \mathbf{u}_pwr^K$ of $\mathbf{G}_{pwr}$ we form the projection matrix **P** to be applied to the vectorized regular sensor-space covariance matrix computed during the **Preprocessing** step. The projection matrix needs to be formed only once for a given forward model. **Output:** Lastly, we modify sensor-space covariance matrix $\mathbf{C}_x$ by projecting its vectorized version into the K-dimensional subspace capturing most of the variation in the columns of $\mathbf{G}_{pwr}$. We then reshape the projected vector back into the matrix form and apply the spectral flip approach (Duin and Pekalska, 2010) to ensure non-negative definiteness of the resulting matrix $\mathbf{C}_x^{abs}$. We then use $\widetilde{\mathbf{C}}_x^{abs}$ instead of $\mathbf{C}_x$ in (3) and (5) to compute the adaptive beamformer weights and output power correspondingly.

in Ossadtchi et al. (2018) where our goal was to suppress the manifestation of volume conduction.

3. Apply the obtained projection matrix **P** to the vectorized sensor-space covariance matrix $vec(\mathbf{C}_x)$ in order to project it onto the source power subspace and reduce the contribution of the components modulated by the off-diagonal elements of the source-space covariance matrix. The projected matrix is then

$$\widetilde{\mathbf{C}}_x = vec^{-1}\left(\mathbf{P} \cdot vec(\mathbf{C}_x)\right). \tag{11}$$

4. The projection procedure followed by reshaping returns a symmetric matrix, see below. However, the projection procedure does not guarantee the positive definiteness of the resulting matrix $\widetilde{\mathbf{C}}_x$ and we ensure this property by replacing its negative eigenvalues with their absolute values. This operation is inline with spectral flip approach introduced in Duin and Pekalska (2010) which has to be used carefully. See Section 3.2.3 for further analysis. Thus, we calculate the final data covariance matrix with suppressed source covariance component contribution from the source-covariance of the correlated sources as

$$\widetilde{\mathbf{C}}_x^{abs} = \widetilde{\mathbf{E}}|\widetilde{\mathbf{\Lambda}}|\widetilde{\mathbf{E}}^T, \tag{12}$$

where $\widetilde{\mathbf{E}}$ and $\widetilde{\mathbf{\Lambda}}$ are the matrices containing eigenvectors and eigenvalues of the matrix after the projection $\widetilde{\mathbf{C}}_x$ and $|\cdot|$ denotes element-wise absolute value. In Section 3.2.3 using the examples of real data covariance matrices we explore in greater detail the issue with non-positive eigenvalues in the post-projected matrix.

5. Use projected covariance matrix $\widetilde{\mathbf{C}}_x^{abs}$ in (3) instead of the original $\mathbf{C}_x$ to compute spatial filters $\mathbf{b}_i$, in (4) to reconstruct the source ac-

tivation timeseries and in (5) to estimate the source power σ_i distribution.

We can prove the symmetry of $\widetilde{\mathbf{C}}_x$, if we realize that M^2-dimensional vector $vec(\mathbf{C}_x)$ projected onto the K-dimensional principal subspace of $\mathbf{G}_{pwr} = \{vec(\mathbf{g}_n\mathbf{g}_n^T)\}$, $n = 1, ..., N$ is a linear combination of K left singular vectors $\mathbf{u}_k$ of $\mathbf{G}_{pwr}$. Since each singular vector is simply a linear combination of the columns of $\mathbf{G}_{pwr}$ we can write that $\mathbf{P} \cdot vec(\mathbf{C}_x) = \sum_{k=1}^{K} \alpha_k \mathbf{u}_k = \sum_{k=1}^{K} \alpha_k \left(\sum_{n=1}^{N} \beta_n^k \cdot vec(\mathbf{g}_n\mathbf{g}_n^T)\right)$. Reshaping this expression back into $M \times M$ matrix form results into a summation of scaled symmetric matrices $\mathbf{g}_n\mathbf{g}_n^T$ that are symmetric itself. Similar arguments can be made to prove that the Whitened ReciPSIICOS projection described next also leads to a symmetric matrix. Therefore, the eigenvalues of this matrix are real numbers.

In vector diagrams in Fig. 2 we show the decomposition of data covariance $\mathbf{C}_x$ as a summation of components from S_{pwr}^K and S_{cor}^K subspaces of the M^2-dimensional space. These principal subspaces are not orthogonal. After projection performed at Step 2 the contribution from S_{cor}^K to $\widetilde{\mathbf{C}}_x$ is supposed to be reduced and the components projecting into S_{pwr}^K are to be left intact.

The ReciPSIICOS procedure of source reconstruction is schematically shown in Fig. 3 for the case of ERP analysis. We use MEG data projected into the forward model principal subspace defined as the subspace capturing 90% of the energy in the forward operator matrix. This allows reducing the number of dimensions to about $60 - 80$ virtual sensors. Following the preprocessing, we split the data into the epochs according to the timestamps of the stimulus onsets. Next, we calculate average

evoked response (ERP). We then use these average ERPs to compute sensor-space covariance matrix. At this step, we have to make sure that the ERP curve is of sufficient length and that our data covariance matrix is full rank.

We follow the steps listed in the beginning of this section to prepare projection operator based on the forward model matrix corresponding to the virtual sensors. This has to be done only once for a given forward model matrix. If the forward model matrix needs to be recomputed for some reason, the ReciPSIICOS projector has to be recalculated.

We then apply this projection operator to the vectorized data covariance matrix and reshape the result of the projection to a square matrix and heuristically fix negative eigenvalue problem as described above. Our experience shows that contribution of the eigendirections modulated by the negative eigenvalues is quite slim and does not exceed 20% of the total energy in the eigenvalue spectrum of the projected matrix, (see section 3.2.3) In our view the proposed heuristics provides an adequate balance of efficiency and simplicity as compared to the full blown consideration of Riemannian geometry of the correlation matrices, which nevertheless constitutes an interesting direction for further improvement of our method. In this section we have described a simple projection into the power subspace. This method delivers a reasonable performance and provides adaptive beamforming scheme with immunity to the source-space correlations inevitably present in the MEG and EEG data. See Section 3 for description of simulations and real-data analysis results where we refer to this method as ReciPSIICOS.

Because S_{pwr}^K and S_{cor}^K non-trivially overlap, the described projection procedure depletes power from both subspaces, but does so at a faster pace for S_{cor}^K subspace. The ultimate balance between the power in the two subspaces achieved with specific value of projection rank K may serve as a quality metric for the procedure. We use these considerations in Section 2.4 where we suggest a strategy for choosing optimal projection rank.

In what follows we will describe another, slightly more complicated procedure, that allows achieving a better balance between the depletion ratio of power in the S_{pwr}^K and S_{cor}^K subspaces.

2.3.3. Whitened ReciPSIICOS projection

Projector **P** built according to the second approach directly projects the vectorized sensor-space covariance *away* from the subspace that captures dominant variance modulated by the source-space correlations. This is done by first estimating the K dimensional principal correlation subspace S_{cor}^K that captures most of the power in the collection of $vec\left(\mathbf{g}_i\mathbf{g}_j^T + \mathbf{g}_j\mathbf{g}_i^T\right), i, j = [1, \ldots, N]$ vectors and then projecting the covariance matrix away from S_{cor}^K. However, in order to maximally spare the source power terms from this projection we operate this projection in the space whitened with respect to S_{pwr}^K. In what follows we refer to this method as Whitened ReciPSIICOS. Step-by-step algorithm of building and applying the whitened projector is presented below as well as the schematic representation in Fig. 4.

1. Construct matrix $\mathbf{G}_{cor}$ whose columns span correlation subspace S_{cor}. The columns of this matrix contain vectorized sums of symmetric source topographies outer-products for all $\frac{N(N-1)}{2}$ ordered pairs of sources. Using $\mathbf{q}_{ij} = vec\left(\mathbf{g}_i\mathbf{g}_j^T\right) = \mathbf{g}_i \otimes \mathbf{g}_j^T$ shortcut form matrix

$$\mathbf{G}_{cor} = [\ldots, \mathbf{q}_{ij} + \mathbf{q}_{ji}, \ldots] \tag{13}$$

and calculate matrix $\mathbf{C}_{cor} = \mathbf{G}_{cor}\mathbf{G}_{cor}^T$.

2. Construct matrix $\mathbf{G}_{pwr}$ whose columns span power subspace S_{pwr}. Columns of this matrix are the vectorized sums of source topography vectors as in the previous projector

$$\mathbf{G}_{pwr} = [\mathbf{q}_{11}, \ldots, \mathbf{q}_{ii}, \ldots, \mathbf{q}_{NN}] \tag{14}$$

Then calculate the matrix $\mathbf{C}_{pwr} = \mathbf{G}_{pwr}\mathbf{G}_{pwr}^T$.

3. Using eigendecomposition of $\mathbf{C}_{pwr}$, compute the whitening operator $\mathbf{W}_{pwr}$ for the source power subspace S_{pwr}

$$\mathbf{W}_{pwr} = \mathbf{E}_{pwr}\mathbf{\Lambda}_{pwr}^{-1/2}\mathbf{E}_{pwr}^T, \tag{15}$$

where $\mathbf{E}_{pwr}$ is the matrix of eigenvectors of $\mathbf{C}_{pwr}$ and diagonal matrix $\mathbf{\Lambda}_{pwr}$ contains the corresponding eigenvalues.

4. Apply whitening transformation to $\mathbf{C}_{cor}$ to obtain $\mathbf{C}_{cor}^w = \mathbf{W}_{pwr}\mathbf{C}_{cor}\mathbf{W}_{pwr}^T$.

5. Extract the principal subspace of $\mathbf{C}_{cor}^w$ by means of eigenvalue decomposition as

$$\mathbf{C}_{cor}^w = \mathbf{E}_{cor}^w \mathbf{\Lambda}_{cor}^w \left(\mathbf{E}_{cor}^w\right)^T \tag{16}$$

6. Form matrix projecting away from the source correlation subspace S_{cor} and operating in the space whitened with respect to S_{pwr}

$$\mathbf{P} = \mathbf{W}_{pwr}^{-1}\left(\mathbf{I} - \mathbf{E}_{cor}^{wK}\left(\mathbf{E}_{cor}^{wK}\right)^T\right)\mathbf{W}_{pwr}, \tag{17}$$

where **I** is identity matrix, $\mathbf{E}_{cor}^{wK}$ is the matrix of the first K eigenvectors of matrix $\mathbf{C}_{cor}^w$, $\mathbf{W}_{pwr}$ is the whitening matrix computed earlier and K is the projection rank and the only parameter in the introduced algorithm that needs to be chosen manually.

7. Apply the obtained matrix **P** to the vectorized sensor-space covariance matrix $vec\left(\mathbf{C}_x\right)$ in order to project it away from the principal source correlations subspace and thus reduce the contribution of the components modulated by the off-diagonal elements of the source-space covariance matrix. The projected matrix is then

$$\widetilde{\mathbf{C}}_x = vec^{-1}\left(\mathbf{P} \cdot vec\left(\mathbf{C}_x\right)\right) \tag{18}$$

8. Again, as with constructing the first projection it can be proved that the projected matrix is symmetric. Also, since this whitened projection procedure does not guarantee the positive definiteness of the resulting matrix $\widetilde{\mathbf{C}}_x$, we ensure this by replacing its negative eigenvalues with their absolute values. In other words, we calculate the final data covariance matrix that has the contribution of the correlated sources suppressed as

$$\widetilde{\mathbf{C}}_x^{abs} = \widetilde{\mathbf{E}}|\widetilde{\mathbf{\Lambda}}|\widetilde{\mathbf{E}}^T, \tag{19}$$

where $\widetilde{\mathbf{E}}$ and $\widetilde{\mathbf{\Lambda}}$ are the matrices containing eigenvectors and eigenvalues of $\widetilde{\mathbf{C}}_x$.

9. Use the projected covariance matrix $\widetilde{\mathbf{C}}_x^{abs}$ in (3) instead of the original $\mathbf{C}_x$ to compute the spatial filters $\mathbf{b}_i$ to reconstruct the source activation timeseries (4) and to estimate the source power σ_i^2 distribution in (5).

Note that this projection is still conceptually complementary to the original PSIICOS (Ossadtchi et al., 2018), as it projects the vectorized covariance *away* from the K-dimensional principal subspace S_{cor}^K computed using the columns of $\mathbf{G}_{cor}$.

Both projection operations will inevitably affect both subspaces. However, as it has been demonstrated earlier in Ossadtchi et al. (2018), the use of spectral value decomposition procedure (SVD) allows identifying a low dimensional subspace of S_{pwr}^K or S_{cor}^K capturing most of the power of the auto-product terms $vec\left(\mathbf{g}_i\mathbf{g}_i^T\right), i = [1, \ldots, N]$ and the cross-product terms $vec\left(\mathbf{g}_i\mathbf{g}_j^T + \mathbf{g}_j\mathbf{g}_i^T\right), i, j = [1, \ldots, N]$.

As in the previous case, this projection procedure is designed without taking into account the Riemannian geometry of the manifold of the correlation matrices. Interestingly, this approach is based on projecting the original vectorized covariance matrix away from S_{cor} yields even smaller fraction of negative eigenvalues. In our experience, this whitened projection operator consistently results into less than 20% of the total energy in the eigenvalue spectrum of the projected matrix.

2.4. Optimal projection rank

In the previous sections we introduced two projection procedures aimed at suppressing the contribution of the components modulated by the off-diagonal elements of the source-space covariance matrix. The projection procedures require only one parameter, the projection rank, that has to be preset by the operator. Since the projection depends only on the forward model, a possible solution is to select the projection rank K based on the simulations like the ones described in Section 3.1.
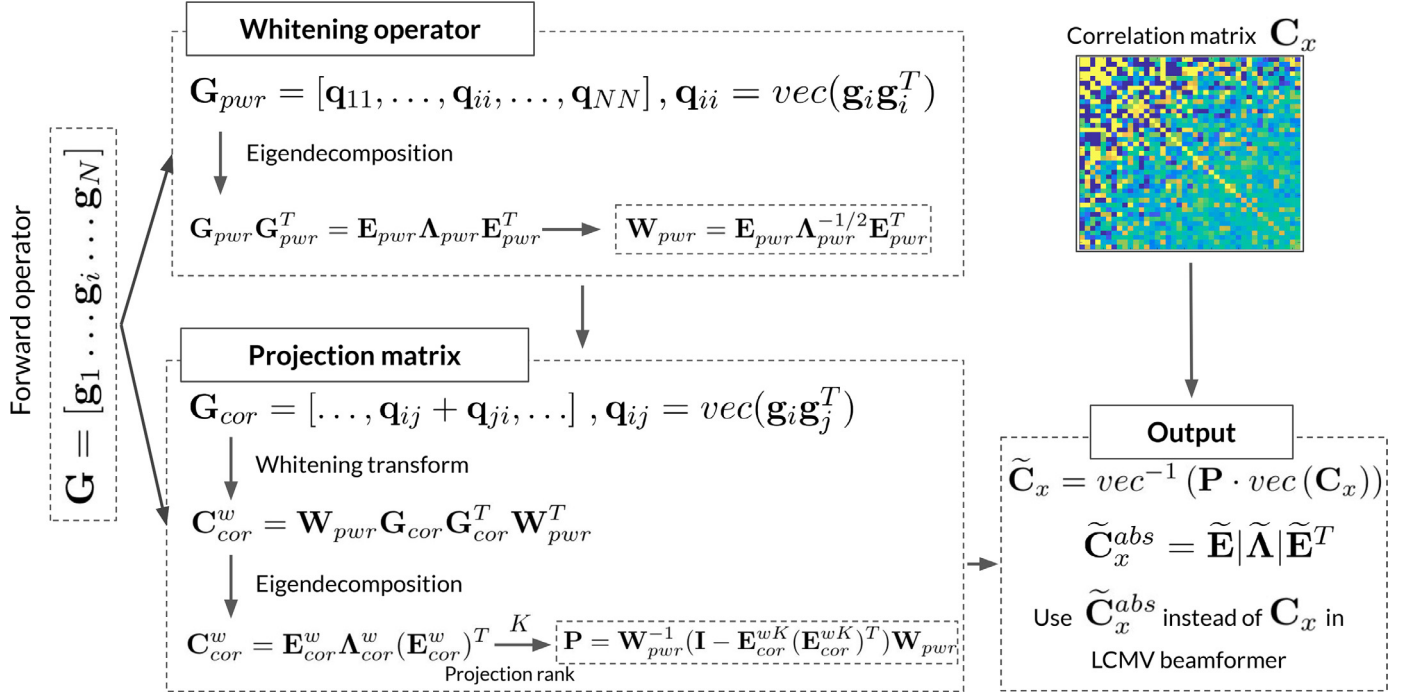
Fig. 4. Schematic presentation of the Whitened ReciPSIICOS algorithm.

The other approach is based on the following considerations. We operate in the M^2-dimensional space and consider Eq. (8) as the observation equation of the $vec(\mathbf{C}_x)$. This equation represents $vec(\mathbf{C}_x)$ as a superposition of activity of sources with the topographies $\mathbf{q}_{ii} = vec(\mathbf{g}_i \mathbf{g}_i^T)$, $i = 1, \ldots, R$ and $\mathbf{h}_{ij} = vec(\mathbf{g}_i \mathbf{g}_j^T + \mathbf{g}_j \mathbf{g}_i^T)$, $i = 1, \ldots, R$, $j = (i+1), \ldots, R$. Vectors $\mathbf{q}_{ii}$ and $\mathbf{h}_{ij}$ mainly project into S_{pwr}^K and S_{cor}^K subspaces correspondingly. To calculate maximum possible energy in each of the subspaces we can assume that the "sources" with "topographies" $\mathbf{q}_{ii}$ and $\mathbf{h}_{ij}$ are activated with unit independent activations and then the total energy in both subspaces can be measured as the trace of the $M^2 \times M^2$ correlation matrices $\mathbf{C}_{pwr}$ and $\mathbf{C}_{cor}$ introduced earlier in Section 2.3.3. After the projection procedure of rank k is performed by means of matrix $\mathbf{P}_k$, the subspace correlation matrices of the observable $vec(\widetilde{\mathbf{C}}_x)$ will read as $\mathbf{P}_k \mathbf{C}_{pwr} \mathbf{P}_k^T$ and $\mathbf{P}_k \mathbf{C}_{cor} \mathbf{P}_k^T$. The fraction of power left in both subspaces can be then computed as

$$P_{pwr}(k) = \frac{trace(\mathbf{P}_k \mathbf{C}_{pwr} \mathbf{P}_k^T)}{trace(\mathbf{C}_{pwr})} \tag{20}$$

and

$$P_{cor}(k) = \frac{trace(\mathbf{P}_k \mathbf{C}_{cor} \mathbf{P}_k^T)}{trace(\mathbf{C}_{cor})} \tag{21}$$

Based on these equations we can plot the curves $(P_{pwr}(k), P_{cor}(k))$ parameterized by projection rank parameter k. An example of such a plot is shown in Fig. 5 that depicts the fraction of past projection power in both subspaces parameterized by the projection rank k.

With the reduction of projection rank in the ReciPSIICOS procedure that performs projection onto the power subspace, more power is depleted from both the subspaces S_{pwr}^K and S_{cor}^K. Conversely, the Whitened ReciPSIICOS implements the projection away from the correlation subspace, so the power is suppressed while the projection rank grows.

Our method works because there exists a range of projection rank values, where the power is depleted faster from the correlation subspace than from the power subspace, i.e. $\delta_P = \frac{dP_{cor}}{dk} - \frac{dP_{pwr}}{dk} > 0$. However, when projection rank k reaches a certain value K^*, the rate of depletion of power from the two subspaces become comparable. Consequently, for the values of $k > K^*$, the difference δ_P changes its sign to negative, i.e. the power subspace starts to lose power faster than the correlation subspace. This projection rank value K^* can be considered

as optimal. Our simulations show that the projection operation remains fairly stable for a broad range of projection rank values k. Yet, these values are affected by the number of virtual sensors used and would significantly differ for different MEG probes.

Fig. 5 demonstrates the power suppression curves for the two proposed methods and for the two MEG arrays: 204-gradiometer array of Neuromag Vectorview-306 (panel A) and 275 gradiometer array of CTF (panel C). In both cases, the number of virtual sensors was selected so that their leadfiled matrix captured 99% of variance present in the original leadfield matrix which resulted into $M^{Nmg} = 50$ and $M^{CTF} = 42$ number of sensors. Panels B and D show the logarithm of marginal gain, defined as $\log(dP_{cor}/dk) - \log(dP_{pwr}/dk)$, as a function of projection rank. According to the imposed assumptions, the optimal projection rank is the value which sets the logarithm of marginal gain in power depletion to zero, which also means that the angle of the tangent to power suppression curve equals to 45° at this point.

This approach demonstrates the clear superiority of Whitened ReciPSIICOS method over plain ReciPSIICOS, as for each value of preserved power in S_{pwr}^K Whitened ReciPSIICOS suppresses more power in S_{cor}^K.

2.5. Handling unknown source orientations

Anatomically, the dipole orientations coincide with the direction of apical dendrites of the pyramidal neurons and therefore are predominantly orthogonal to the cortical mantle.

Modern tools of MRI data analysis allow for a very accurate extraction and precise parametrization of the cortical surface with the number of nodes on the order of several hundreds of thousands, which in turn results in a reasonable accuracy of the orientation specification. However, in practice significantly sparser grids of tens of thousands of nodes are used which leads to the increased uncertainty in the orientation parameter. To compensate for this it is customary to place a triplet of dipoles in each node to accommodate any orientation to be learnt from the data. The local forward matrix is then represented by a triplet of topographies corresponding to the three dipoles. As shown in Ahlfors et al. (2010), even with realistically shaped forward models the third dimension in the node forward model conveys to the data median 6% of energy of the local source with the most powerful orientation. Based on this, we follow the common practice in MEG inverse modelling and reduce local
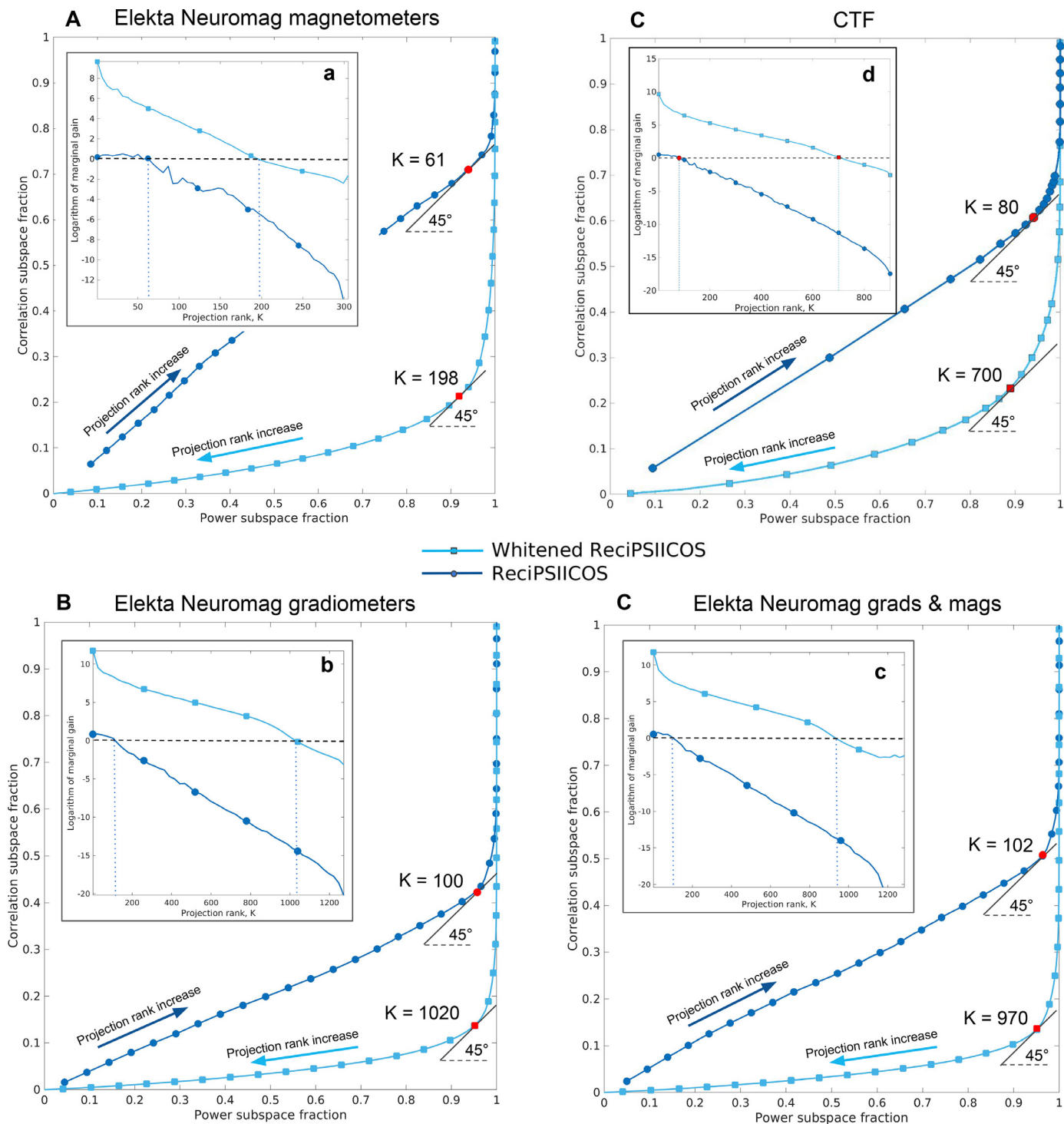
Fig. 5. Parametric curves of power depletion in the S_{pwr} and S_{cor} subspaces parameterized by projection rank for ReciPSIICOS and Whitened ReciPSIICOS projections for Elekta Neuromag 102 magnetometers array (panel A), 204 gradiometers (panel B) and 306 magnetometers and gradiometers (Panel C) and and 275 radial gradiometers CTF array (panel D). The inserts show the logarithm of marginal gain, $\log(dP_{cor}/dk) - \log(dP_{pwr}/dk)$, as a function of projection rank. The optimal projection rank is the value which sets the logarithm of marginal gain in power depletion to zero, which corresponds to the 45° angle of power suppression curves tangent.

forward matrix dimension to two (Mosher et al., 1999). While this represents a working solution, it is important to keep in mind that in some deep cortical and subcortical regions the fraction of energy contributed by the third dimension can be as high as 20% which may potentially improve spatial resolving power of MEG given that the forward modeling accuracy is preserved for these typically deep regions.

For an arbitrary orientation vector at some i-th vertex $\boldsymbol{\theta}_i = [\theta_i^x, \theta_i^y]^T$, the corresponding dipole topography is $\mathbf{g}_i^{\theta_i} = [\mathbf{g}_i^x, \mathbf{g}_i^y]\boldsymbol{\theta}_i$, where $\mathbf{g}_i^x, \mathbf{g}_i^y$ are the topographies of the two orthogonally oriented dipoles in the tangential plane at the i-th vertex. By varying the orientation angle we can obtain an infinite set of power subspace topography vectors $vec(\mathbf{g}_i^{\theta_i}(\mathbf{g}_i^{\theta_i})^T)$!

Expanding these auto-products of topographies of the oriented dipoles in terms of the topographies $\mathbf{g}_i^x$, $\mathbf{g}_i^y$, $i = [1, \ldots, N]$ oriented along x and y axis of the local tangential plane we obtain

$$vec\left(\mathbf{g}_i^{\theta_i}(\mathbf{g}_i^{\theta_i})^T\right) = \mathbf{g}_i^{\theta_i} \otimes \mathbf{g}_i^{\theta_i} = (\mathbf{G}_i \theta_i) \otimes (\mathbf{G}_i \theta_i)$$
$$= (\theta_i^x)^2 \mathbf{g}_i^x \otimes \mathbf{g}_i^x + \theta_i^x \theta_i^y (\mathbf{g}_i^x \otimes \mathbf{g}_i^y + \mathbf{g}_i^y \otimes \mathbf{g}_i^x) + (\theta_i^y)^2 \mathbf{g}_i^y \otimes \mathbf{g}_i^y \tag{22}$$

In the above for compactness we have replaced the operation of vectorized outer product of two vectors with an equivalent operation of Kronecker product of these two vectors since $vec(\mathbf{a}, \mathbf{b}) = \mathbf{a} \otimes \mathbf{b}$.

Therefore, in order to accommodate the arbitrary orientation constraint, elements $\mathbf{g}_i \otimes \mathbf{g}_i$ in Eqs. (9) and (14) have to be replaced by $[\mathbf{g}_i^x \otimes \mathbf{g}_i^x, \ \mathbf{g}_i^x \otimes \mathbf{g}_i^y + \mathbf{g}_i^y \otimes \mathbf{g}_i^x, \ \mathbf{g}_i^y \otimes \mathbf{g}_i^y]$.

Arbitrary orientations lead to a slightly more cumbersome manipulation for the cross-products of topographies. Similarly to the auto-products step sums of vectorized outer-products of topographies of different arbitrarily oriented sources present in Eq. (13) can be expanded using Kronecker product notation as

$$vec\left(\mathbf{g}_i^{\theta_i}(\mathbf{g}_j^{\theta_j})^T\right) + vec\left(\mathbf{g}_j^{\theta_j}(\mathbf{g}_i^{\theta_i})^T\right) = \mathbf{g}_i^{\theta_i} \otimes \mathbf{g}_j^{\theta_j} + \mathbf{g}_j^{\theta_j} \otimes \mathbf{g}_i^{\theta_i} = (\mathbf{G}_i \theta_i) \otimes (\mathbf{G}_j \theta_j)$$
$$+(\mathbf{G}_j \theta_j) \otimes (\mathbf{G}_i \theta_i) = \theta_i^x \theta_j^x (\mathbf{g}_i^x \otimes \mathbf{g}_j^x + \mathbf{g}_j^x \otimes \mathbf{g}_i^x) + \theta_i^x \theta_j^y (\mathbf{g}_i^x \otimes \mathbf{g}_j^y$$
$$+\mathbf{g}_j^y \otimes \mathbf{g}_i^x) + \theta_j^y \theta_i^x (\mathbf{g}_j^y \otimes \mathbf{g}_i^x + \mathbf{g}_i^x \otimes \mathbf{g}_j^y) + \theta_i^y \theta_j^y (\mathbf{g}_i^y \otimes \mathbf{g}_j^y + \mathbf{g}_j^y \otimes \mathbf{g}_i^y). \tag{23}$$

Therefore, elements $vec\left(\mathbf{g}_i^{\theta_i}(\mathbf{g}_j^{\theta_j})^T\right) + vec\left(\mathbf{g}_j^{\theta_j}(\mathbf{g}_i^{\theta_i})^T\right)$ in Eq. (13) are to be replaced with

$$\left[\mathbf{g}_i^x \otimes \mathbf{g}_j^x + \mathbf{g}_j^x \otimes \mathbf{g}_i^x, \ \mathbf{g}_i^x \otimes \mathbf{g}_j^y + \mathbf{g}_j^y \otimes \mathbf{g}_i^x, \ \mathbf{g}_i^y \otimes \mathbf{g}_j^x \right.$$
$$\left. +\mathbf{g}_j^x \otimes \mathbf{g}_i^y, \ \mathbf{g}_i^y \otimes \mathbf{g}_j^y + \mathbf{g}_j^y \otimes \mathbf{g}_i^y \right].$$

The rest of the procedure for building the projector is unaltered.

2.6. Monte Carlo simulations

In order to compare the proposed algorithms with other relevant source reconstruction methods we ran several Monte Carlo simulations. To simulate the MEG signals, we used cortical surface model with 20000 vertices reconstructed from anatomical MRI data using FreeSurfer software (Fischl, 2012). The forward model matrix $\mathbf{G}$ for freely oriented dipolar sources was computed with Brainstorm software (Tadel et al., 2011) using the overlapping spheres procedure. Each location on the cortical grid was served by two topography vectors confined to the locally tangential plane as determined by the first two right singular vectors of the local $[M \times 3]$ forward matrix.

In different experiments, we studied the interaction of two or three sources. For each Monte Carlo trial, a random set of pairs or triplets of dipolar sources was picked as the target stimulus-related sources. One hundred epochs were generated and then averaged to obtain the event related field (ERF). The activations of target sources $\mathbf{s}(t)$ were modeled with 10-Hz sinusoids.

The simulated data mimicked two experimental conditions: the first with highly correlated source activation timeseries and the second with uncorrelated ones. To model these two extreme cases, the phase difference between activation timeseries was set to zero for the correlated condition and to $\frac{\pi}{2}$ for the uncorrelated condition. Each trial onset was jittered with respect to the task onset by adding a random shift generated from zero-mean normal distribution with the standard deviation corresponding to $\frac{\pi}{8}$ phase difference.

We modeled task irrelevant activity with 1000 task-unrelated cerebral sources whose locations and timeseries varied with each epoch. Source locations were mapped on the nodes of the high resolution cortical grid (20000 vertices). The activation timeseries were narrow-band signals obtained via zero-phase filtering of the realizations of Gaussian (pseudo)random process by the fifth order band-pass IIR filters in the bands corresponding to theta (4-7 Hz), alpha (8-12 Hz), beta (15-30 Hz)

and gamma (30-50 Hz, 50-70 Hz) activity. Their relative contributions were scaled in accordance with the well-known $1/f$ characteristic of the MEG spectrum. We scaled the brain noise components to match typical signal-to-noise ratio of real-life recordings. To project these sources into the sensor space, the corresponding columns of the forward matrix was computed for the high resolution source grid. We simulated 100 epochs of ERF data and for each epoch a new randomly picked set of noisy sources was chosen and new noisy timeseries with approximately $1/f$ spectrum were generated. We defined the SNR in our simulated data in the sensor space as the ratio of Frobenius norms of data matrices for the induced and brain noise components filtered in the band of interest (0.5-7 Hz), corresponding to the ERF response.

We did not perform whitening of the data (and the model) with respect to noise covariance $\mathbf{C}_n$. In the ERP setting this covariance could be estimated from a small number of samples over the pre-stimulus interval. Whitening with respect to such a noisy covariance estimate would require regularization for which there is no universally working recipe (Engemann and Gramfort, 2014). Also, the whitening changes the forward operator which would then require recomputing ReciPSIICOS and Whitened ReciPSIICOS projections. The former is fast and the latter is way slower and takes about 5-10 minutes on a regular PC and normally needs to be done once per forward model. However, in the case of 500 Monte-Carlo simulations per condition with new noise samples on every MC trial this would result into a very significant computational burden that we decided to avoid. Given that the proper whitening may improve the source localization accuracy, the results reported here for the low SNR cases can be conservative.

The high resolution grid of 20,000 vertices was used only for data simulation. For the source reconstruction process we employed a 4 times sparser cortex grid with 5000 vertices. Both projectors (10) and (17) were computed using the sparser grid. We ran 500 simulations and compared two versions of the proposed ReciPSIICOS method against the classical adaptive vector LCMV beamformer (Sekihara et al., 2001) and MNE techniques.

We have also projected the data into the principal subspace capturing 95% of variance in the forward model matrix. This helps us to improve the condition number of data covariance matrices. In addition, we follow a safe strategy and augment matrix inversions with a simple Tikhonov regularization, however, the regularization parameters are usually very small and fall into $10^{-3} - 10^{-2}$ range.

2.7. Performance metrics

In our Monte Carlo simulation analysis, goodness of localization was estimated using three metrics: source localization bias, point spreading radius and ratio of successful detection. While the data were simulated using dense cortical model with 20,000 sources, source reconstruction procedure was based on the sparse cortical model with 5000 sources to make the reconstruction procedure more realistic. We considered separately the scenarios with two and three target sources. In order to run the comparative analysis for each Monte Carlo trial we repeated the following steps:

1. Given the simulated data with target sources $\mathbf{r}_0^j = [x_j, y_j, z_j]$, where $j = \{1, \ldots, N_{src}\}$ for number of sources $N_{src} = 2$ or $N_{src} = 3$, estimate the power of each source $\mathbf{Z} = [z^1, \ldots, z^M]$ using the four studied methods (ReciPSIICOS, Whitened ReciPSIICOS, LCMV, MNE). The sources with estimated power below the threshold α are considered as inactive. α is computed as a fraction of maximal estimated power value among all sources as $\alpha = a \cdot \max(\mathbf{Z})$, $0 \leq a \leq 1$. To mimic real-life situation, we choose the parameter a individually for each Monte Carlo iteration and each method, according to the following procedure. We scan through the grid of different values of a. Each threshold value results in a specific number of connected regions (clusters). We then choose the highest value of the threshold that results into the number of sources that were simulated N_{src}. In case we can

not find such a threshold value, we repeat the above procedure for $N_{src} - 1$ sources. Sources with estimated power exceeding α are considered as active and assigned to the closest target source in terms of the Euclidean distance.

2. All active sources are divided into C clusters $\mathbf{S}^{cl} = \{\mathbf{r}_1^{cl}, \dots, \mathbf{r}_{N^{cl}}^{cl}\}$, $cl = \{1 \dots C\}$, $C \leq N_{src}$, according to their correspondence to one of the target sources, where N^{cl} is the number of sources in each cluster. In each cluster find the source with maximal estimated power

$$(\mathbf{r}^*)^{cl} = \mathrm{argmax}_j(\mathbf{Z}(\mathbf{r}_j^{cl})),$$

where $j \in 1 \dots N^{cl}$, $cl = \{1, 2\}$ or $cl = \{1, 2, 3\}$.

3. Calculate the average Euclidean distance between the local maxima in each cluster and the corresponding target source. The obtained value reflects the source localization bias and is measured in meters:

$$B = \frac{1}{C} \sum_{cl=1}^{C} \|(\mathbf{r}^*)^{cl} - \mathbf{r}_0^{cl}\|^2$$

4. To estimate the point spreading radius, first normalize the estimated power values inside each cluster

$$\widetilde{\mathbf{Z}}(\mathbf{r}_j^{cl}) = \frac{\mathbf{Z}(\mathbf{r}_j^{cl})}{\sum_{j=1}^{N^{cl}} \mathbf{Z}(\mathbf{r}_j^{cl})},$$

where $j \in 1 \dots N^{cl}$, $cl = \{1 \dots C\}$, and then calculate the distance between each source belonging to the current cluster and the source with maximal estimated power. The point spreading radius is then the averaged sum of computed distances weighted with the normalized power values

$$PS = \frac{1}{C} \sum_{cl=1}^{C} \sum_{j=1}^{N^{cl}} \widetilde{\mathbf{Z}}(\mathbf{r}_j^{cl}) \|\mathbf{r}_j^{cl} - (\mathbf{r}^*)_i^{cl}\|^2.$$

5. If the number of detected clusters C is lower than the number of modeled sources (2 or 3), this simulation is considered as an unsuccessful detection. Also, if the source localization bias is higher than 2 cm, which means that the peak of reconstructed activity is 2 cm away from the initial location, this case is also considered as an unsuccessful detection. The detection ratio is then defined as the ratio of successful detection across all simulations.

For all simulations, we computed statistical distributions of the metrics of interest and the corresponding median values. We used localization bias and point spreading area as accuracy metrics for each method.

The described procedure and considered metrics give the highly intuitive output and result into criteria which are usually used in the manual expert evaluation of source reconstruction results. Moreover, the obtained characteristics of LCMV and MNE reconstruction perfectly fit the previous results (Rana et al., 2018), which also confirms the consistency of the chosen metrics.

2.8. MEG data acquisition and handling

We applied the ReciPSIICOS and Whitened ReciPSIICOS algorithms to the MEG datasets from two experiments that involved auditory processing. The behavioral tasks and MEG recording systems were different in these experiments.

2.8.1. Dataset 1

The first dataset contained MEG data for one healthy subject and one ASD patient. The data were collected at Moscow MEG facility with Elekta-Neuromag Vectorview 306 system (Elekta Oy, Finland) with 204 planar gradiometers and 102 magnetometers. The subjects participated in a passive listening session. During the experiment, the 40 Hz auditory stimuli sequence was presented monaurally in the left ear. The session consisted of 80 trials. MEG data were recorded with 1000 Hz sampling frequency. The data were preprocessed using the Elekta MaxFilter™ software that performs spatial and temporal projections to suppress

data components emanating from sources with the origin outside the sphere inscribed into the MEG helmet inner border, see (Taulu and Simola, 2006) for technical details and (Nenonen et al., 2012) for a study exploring the effects of MaxFilter™ on the ERF data.

To compute the auditory steady-state responses (ASSR), we considered the low gamma-band oscillations as the primary focus of the analysis. The preprocessed data were band-pass filtered in the 35–45 Hz band using a band-pass FIR filter with 128 taps. The obtained signals were epoched 500 ms prior- and 1 s post-stimulus and averaged to obtain the ERF.

The sensor-space covariance matrix was computed for the average ERF. The length of the ERF timeseries (including the pre-stimulus interval) was 1.5 s (1500 samples) for the virtual sources count of $M = 50$. This number of samples was sufficient for the estimation of the sensor-space covariance matrix. Based on the individual 1.5 T MRI scans forward model, matrices comprising topographies of freely oriented dipoles in the 20,000 mesh grid nodes were calculated individually for the two participants.

2.8.2. Dataset 2

The second dataset was collected in one subject using a CTF-275 MEG system. The data were recorded in the Montreal Neurological Institute, McGill University, Canada by Elizabeth Bock, Peter Donhauser, Francois Tadel and Sylvain Baillet for Brainstorm tutorial (Tadel et al., 2011). The subject received auditory stimuli binaurally through intra-aural earphones (air tubes + transducers). The stimuli included a total of 200 regular beeps (440 Hz) and 40 easy deviant beeps (554.4 Hz, 4 semitones higher). The inter-stimulus interval was randomized and uniformly sampled between 0.7 s and 1.7 s seconds. The subject was in a seating position. He was instructed to press a button with the right index finger when detecting a deviant stimulus. Auditory stimuli were generated with the MATLAB Psychophysics toolbox. MEG data were acquired at 2400 Hz. The data were saved from the CTF acquisition software with the 3-rd gradient correction option.

The anti-aliasing low-pass filter with cutoff frequency of at 600 Hz was applied and the data were saved with the 3-rd order gradient correction option offered by the CTF acquisition software. Eye artifacts were removed using ICA decomposition. The data were bandpass filtered in the 1-70 Hz band using a band-pass FIR filter with 128 taps. The obtained signals were epoched 100 ms prior- and 500 ms post-stimulus and averaged separately for deviant and standard stimuli. To obtain an MMN component, we computed the difference between the deviant and standard responses.

2.8.3. Forward and inverse operators

Forward operators were computed via Brainstorm software (Tadel et al., 2011) using an overlapping spheres model. MNE inverse operator was computed in agreement with its implementation in the Brainstorm software and for LCMV we used vector beamformer formulation (Sekihara et al., 2001). Due to the typically high SNR in the ERF/ERP data, no noise covariance was supplied to either of the algorithms. ReciPSIICOS and Whitened ReciPSIICOS inverse operators, as well as all the simulations and analysis, were performed using custom MATLAB scripts.

3. Results

3.1. Monte Carlo simulation study

The performance of ReciPSIICOS and Whitened ReciPSIICOS projections was tested using Monte Carlo simulations, according to the methodology described in Section 2.6. To perform a comparative analysis for each simulation, the source power was estimated using four techniques discussed above: ReciPSIICOS, Whitened ReciPSIICOS, LCMV and MNE. Simulated data were generated using a dense cortical grid of 20000 sources, and source reconstruction procedure used a four times

sparser cortical model with 5000 sources. This study design allowed to perform a more realistic simulation analysis, though naturally entails small additional persistent bias in all considered metrics.

3.1.1. Two interacting sources

Source reconstruction results for a single trial of Monte Carlo simulations with two active sources are shown in Fig. 6. The left and right panels show the results for the synchronous and asynchronous pairs of sources, correspondingly. For each Monte-Carlo iteration, such as the one depicted in Fig. 6, the pair of symmetrically located dipolar sources was picked randomly. SNR in the ERP corresponding to the simulated data was set to 4. Each subplot on the graph demonstrates cortical distribution of the estimated variance and the scatter plots allow to appreciate the dynamic range of the obtained solutions. As expected, in the case of the asyncronous sources, ReciPSIICOS, Whitened ReciPSI-ICOS and LCMV demonstrated spatially tight activation distributions, while MNE-produced map was characterized by a significantly greater cortical spread. For synchronous sources, the LCMV beamformer clearly showed a signal cancellation effect and completely failed to localize true sources, while the proposed projection remained operable in both ReciPSIICOS and Whitened ReciPSIICOS versions.

It is important to note that, as evident from this single MC-trial example (Fig. 6), the proposed projection did not adversely affect spatial spatial resolution of the beamformer-based inverse solution in the asynchronous case and kept operating in the scenario with synchronous sources whereas the original adaptive LCMV failed to recover the simulated sources. The MNE technique was insensitive to the correlation between sources and showed qualitatively identical results in both synchronous and asynchronous cases. We would also like to point out that the the magnitude of and dynamic range of ReciPSIICOS and Whitened ReciPSIICOS obtained solutions appeared to be noticeably greater than those delivered by the MNE and the LCMV techniques.

As we will show in the later sections, the norms of the inverse operator rows for the LCMV and the two techniques proposed here are of comparable magnitude. Therefore the increased magnitude of the output in both synchronous and asynchronous cases is explained by the proper orientation of the corresponding spatial filter (row of the inverse operator) aimed at emphasizing target source activity and not using activation of synchronous sources to chase the minimum variance requirement. The fact that the increase in magnitude was observed in both synchronous and asynchronous cases can be explained by the fact that the sources present in the realistically simulated brain noise are used by the greedy LCMV solution to further minimize the output variance.

To generalize the observations described above we performed 500 Monte Carlo simulations with 500 trials and used the three metrics detailed in section 2.7: source localization bias, radius of point spreading and ratio of successful detection to compare the performance of the four methods. We investigated the performance for various SNR and forward model inaccuracies and presented them as medians computed over all 500 MC iterations for each condition. To generate the spatially structured perturbation for the forward model matrix we used the head models computed for 10 subjects and calculated the pairwise differences between the forward models for each pair of subjects. We then computed the structured noise matrix as the average of these pairwise differences. We then standardized the resulting structured noise matrix and added it to the true forward model. We adjusted the amount of noise by parameter δ used to scale the noise matrix. The use of a decimated version of the cortex for source localization as compared to the data generation step results into an additional contribution to the forward modelling errors.

Fig. 7 demonstrates the results of comparative analysis of performance as a function of SNR (panel A) and forward model inaccuracies (panel B). Consider first the noise-free forward model operator (panel A). All four methods, except for the adaptive LCMV in the synchronous case, demonstrate stable performance for SNR > 2. In case of uncorrelated source activations, ReciPSIICOS and Whitened ReciPSIICOS, as well as LCMV beamformer, demonstrate high performance: detection

ratio is close to 100%, localized area is compact and coincides with the simulated location. At the same time, MNE demonstrates low localization bias and, as expected, a greater point spreading radius. It detects only one source for 40% of trials MNE. These localization characteristics perfectly fit the findings described in the recent study (Rana et al., 2018).

Considering the right panel of Fig. 7.A, one can see that for correlated signals LCMV performance drops significantly and does not improve with the growing SNR. Due to severe signal cancellation the detection ratio characteristics is below 10%, which means that only in 10% of cases LCMV detects two activation blobs with the maximum value not further than 2 cm from the simulated locations. While the three methods reach equally good localization bias at the level comparable with the uncorrelated case, they can be further analyzed on the basis of the two other quality metrics. Whitened ReciPSIICOS demonstrates noticeably lower radius of spreading at the expense of a slightly reduced detection ratio as compared to the ReciPSIICOS. We can also see that even in the synchronous case both proposed methods outperform the MNE. Fig. 8 demonstrates distribution of the localization bias and point-spreading area for synchronous and asynchronous cases corresponding to SNR = 4 slice of dependencies in 7.A.

Since the performance of all inverse solvers, and those based on the LCMV principle in particular, depends on the forward model inaccuracies, in panel B of Fig. 7 we analyzed the extent to which the inaccuracies in forward modeling affected the three characteristics of the inverse solutions obtained by the four different solvers. For uncorrelated sources, one can observe that the localization bias is low enough for all methods (only slightly higher for MNE) and increases insignificantly with the increase of forward model error. As expected, the area of activity spreading grows for all beamformer-based methods, but remains within the acceptable range for the typical MEG forward model noise levels of 10% (Mosher et al., 1999). MNE's performance appears to be not adversely affected by the explored range of FM inaccuracy levels.

For correlated sources, the performance of ReciPSIICOS pars that of the MNE with a slightly higher detection ratio pertinent to the ReciPSIICOS. The Whitened ReciPSIICOS shows more compact solutions than the other three techniques and a higher detection ratio. In the synchronous case, due to general deterioration of performance of all three beamforming methods, the effects of forward model inaccuracies are significantly less pronounced than in the situation with asynchronous sources.

Projection rank is the only user defined parameter of the ReciPSI-ICOS and Whitened ReciPSIICOS techniques. Fig. 9 depicts the three performance metrics considered above as functions of the projection rank for the two methods in synchronous and asynchronous cases. From these plots, both ReciPSIICOS approaches are characterized by a smooth and relatively flat performance profiles as a function of projection rank. Note that the projection rank has a different meaning for ReciPSIICOS and Whitened ReciPSIICOS. Increased projection for ReciPSIICOS corresponds to a less restrictive situation when the variance from the correlation subspace is expected to leak more intensively into the power-only subspace. At the same time, the greater the projection rank for the Whitened ReciPSIICOS method, the stronger is the suppression of the undesired variance from the correlation subspace, which happens at an expense of the variance in the power-only subspace. These simulations were conducted for the Neuromag probe and agree well with subspace power ratio plots in Fig. 5.

3.1.2. Three interacting sources

The majority of the present solutions to the correlated sources problem in beamforming (see Introduction) handle pairs of correlated sources by suppressing the source correlated with the target one by means of an extra zero constraint. In principle, these existing techniques can be extended to the triplets, quadruplets and etc. of potentially correlated sources. However, such an extension would lead to significant computational demands and would require methods for fusing the ob-
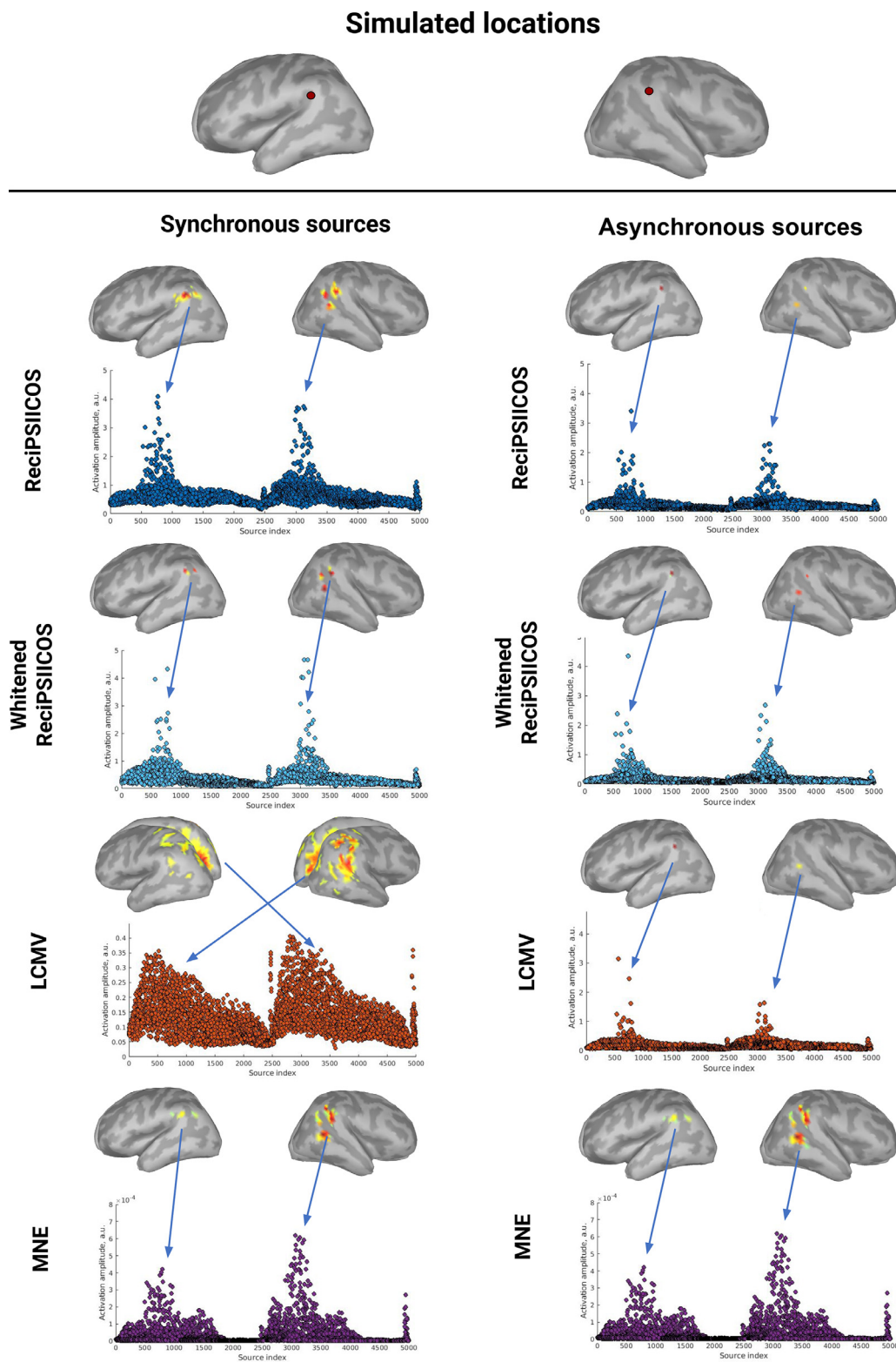
Fig. 6. Estimated source power for one Monte Carlo simulation. The pair of active symmetric sources was picked randomly and activated synchronously (left panel) and asynchronously (right panel). The source reconstruction was performed using four techniques: ReciPSIICOS, Whitened ReciPSIICOS, LCMV and MNE. The noise was set to SNR = 4. Each subplot shows the estimated amplitudes (y-axis, scale is individual) for each of 5000 sources (x-axis).
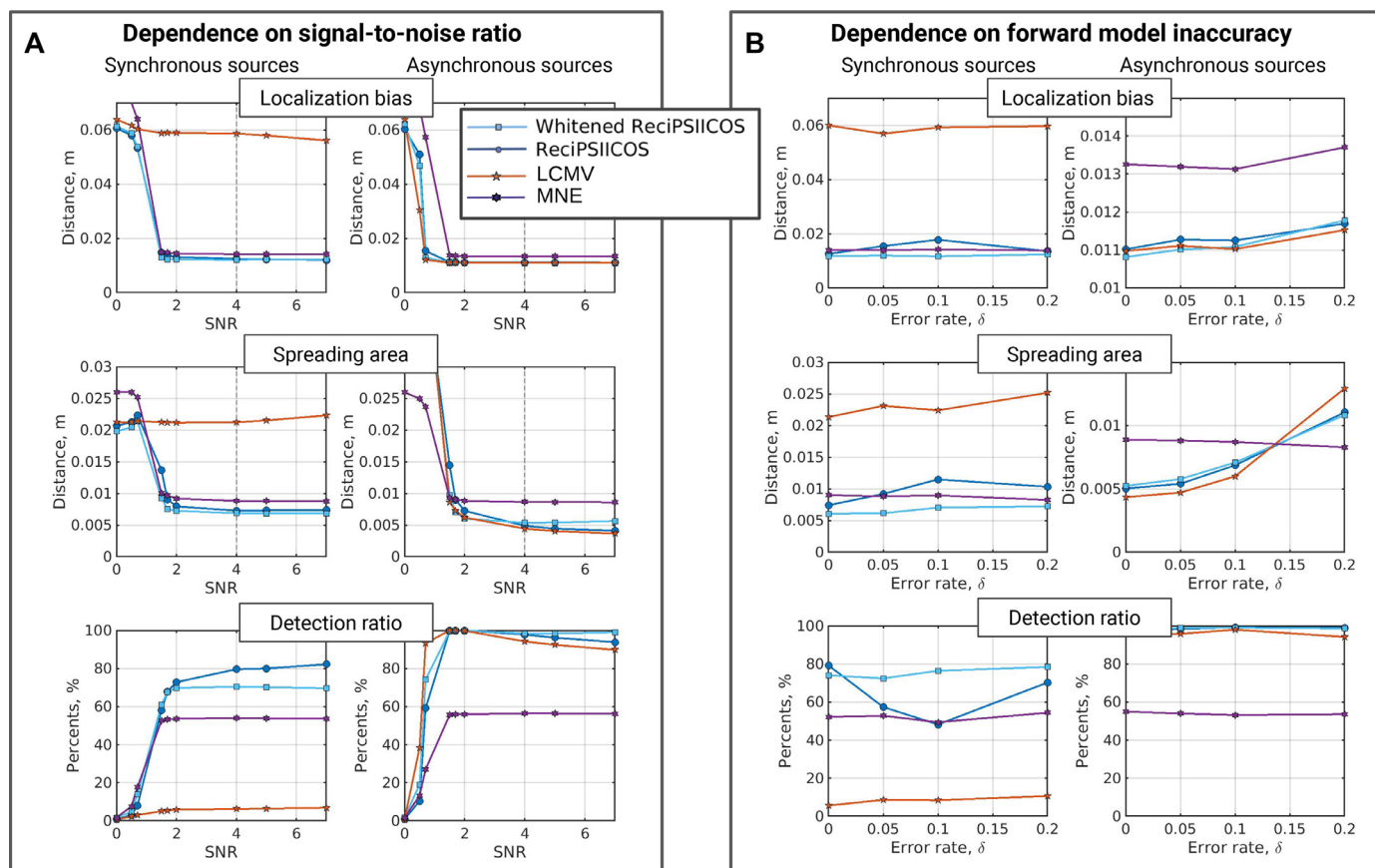
Fig. 7. Monte Carlo simulation study results. Comparison of ReciPSIICOS, Whitened ReciPSIICOS, LCMV and MNE localization for synchronous and asynchronous sources according to three metrics: localization bias, area of point spreading and detection ratio. **A.** Dependence of estimated metrics on SNR. **B.** Dependence of estimated metrics on forward model inaccuracy.

tained results. The approach proposed here takes care of all correlated sources simultaneously. In this section we will focus on the example of three correlated sources. The data were modelled as described in Section 2.6 and the three target sources were picked randomly, but so that they were no closer than 4 cm apart. We first consider sources activated with sinusoidal functions with a zero phase shift, but slightly jittered in time (see Fig. 11.B). A representative case (a single Monte Carlo trial) is shown in Fig. 10. Panel A illustrates locations of three randomly picked sources in the right frontal, right ventral and left parietal areas. We can see that in this scenario the LCMV beamformer produces a completely incorrect activation map, ReciPSIICOS and MNE detect all three sources and demonstrate the comparable results. The Whitened ReciP-SIICOS shows an outstanding performance, as the obtained activations are extremely focal and they successfully capture the initial activity.

These findings are generalized using 500 Monte Carlo trials in Fig. 11. Distribution of localization bias and point spreading radius for different methods over 500 Monte Carlo trials are shown as histograms in Fig. 11.A. Dashed lines depict the median values. According to the first two metrics, it can be concluded that in the case of multiple active sources Whitened ReciPSIICOS significantly outperforms the competing methods, even the simple ReciPSIICOS. ReciPSIICOS and MNE show the similar performance, as we could see previously with two sources. Classical LCMV has the worst performance and basically fails.

Panel C of the Fig. 11 demonstrates the distribution of the number of detected sources, where the first point corresponds to the ratio of all trials when all three ground-truth sources were found. Thus, in 63% of all simulations, Whitened ReciPSIICOS was able to localize all three sources while ReciPSIICOS performance was at 48%, MNE had a slightly lower performance at 44% and LCMV did not find the three sources in any simulation.

Fig. 12 demonstrates the same metrics for the three moderately correlated sources activated with sinusoidal functions with $\frac{\pi}{3}$ relative phase shift. This shift results in 0.5 pairwise correlation. As we can see, LCMV beamformer fails to detect three simulated sources in more than 80% of cases, whereas the methods from ReciPSIICOS family handle this situation well and loose one source only in 20% of cases. The bias and spreading metrics are also superior to the classical methods.

3.2. Real MEG data

In this section we describe the results of applying the proposed methodology to the real MEG datasets taken from two different experiments. The detailed descriptions of the paradigms and the datasets used are provided in Section 2.8.

3.2.1. Dataset 1

In this experiment, subjects received monaural auditory stimuli in the left ear. The following results were computed at a latency of 250 ms post-stimulus corresponding to the maximum amplitude of the response. Figs. 13 and 14 show the estimated source power for both subjects and all considered methods. The source reconstruction revealed, as expected, most prominent activations in superior temporal gyrus, namely primary auditory cortex. Since the left ear received the stimulus, we expected to observe a stronger activation in the contralateral, right hemisphere and a weaker activation in the left hemisphere.

For the first subject (Fig. 13), it can be seen, that ReciPSIICOS, in comparison with LCMV beamformer and MNE, reveals more focal activations with the anticipated distinct maximum in the right auditory cortex and a lower, but still nonzero, activation in the left hemisphere. LCMV beamformer demonstrates a similar ipsilateral activation but an
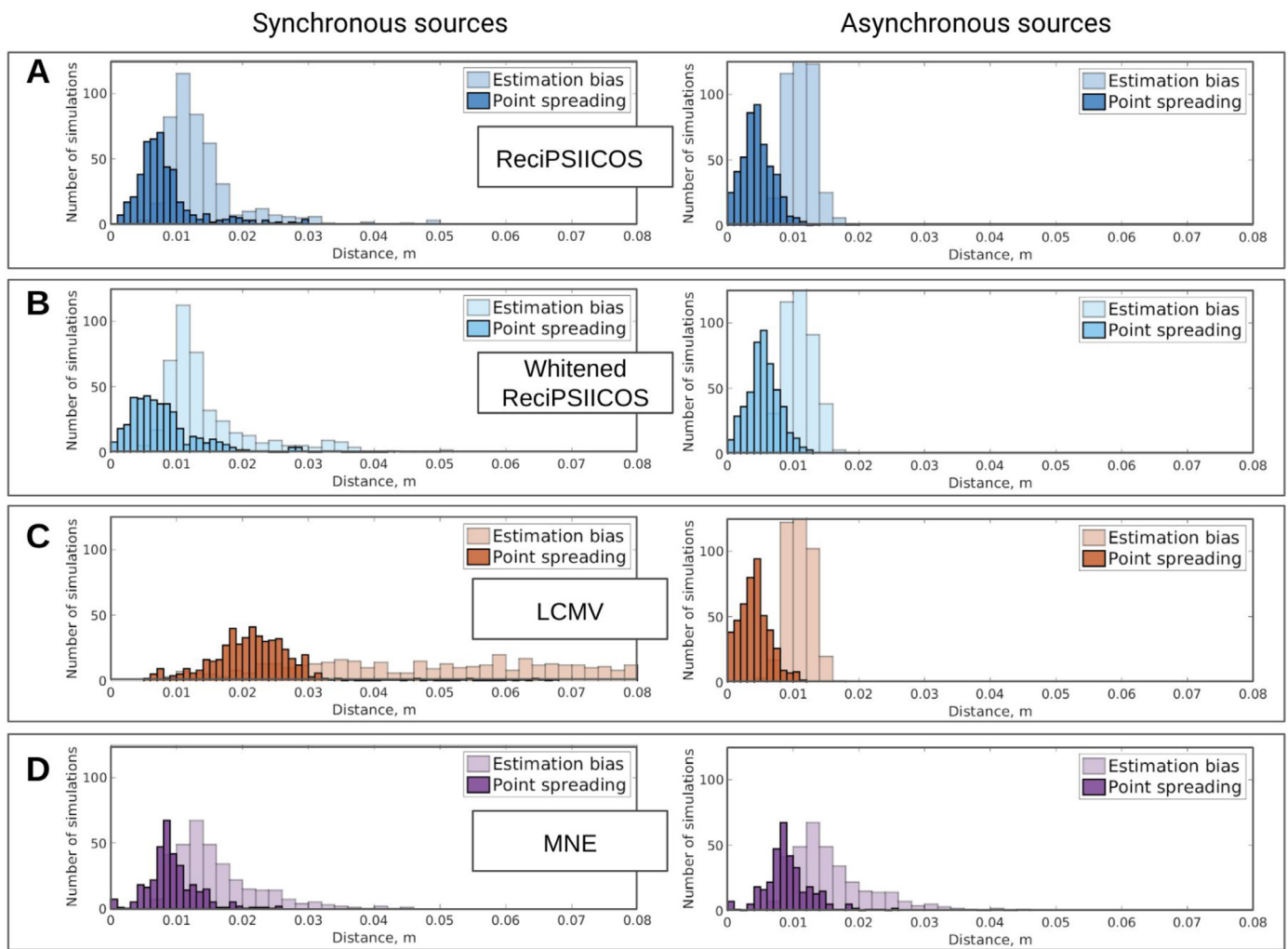
Fig. 8. Distribution of localization bias and area of point spreading metrics for 500 Monte Carlo simulations. Noise level is adjusted so that SNR = 4. The results are computed for ReciPSIICOS (A), Whitened ReciPSIICOS (B), LCMV (C) and MNE (D).

absolutely incorrect contralateral pattern. MNE detects only the right hemisphere blob activation. For this subject, Whitened ReciPSIICOS shows the results similar to the simple ReciPSIICOS, but the latter provides more focal activations. Notably, the amplitudes reconstructed with the LCMV beamformer technique are approximately 400 times lower in the dynamic range than those reconstructed with ReciPSIICOS, with the maximal power of $8 \cdot 10^{-26}$ and $2 \cdot 10^{-24}$ respectively.

The results for the second subject (Fig. 14) are similar to those for the first one. The best localization is demonstrated by ReciPSIICOS, while LCMV does not capture the activity in the contralateral hemisphere and MNE localizes two spreaded activity blobs. Unlike it is the case with MNE, the cortical distributions obtained with both versions of ReciPSIICOS show bilateral focal blobs of activity in the superior temporal regions corresponding to the primary auditory areas. The blobs of activity obtained with ReciPSIICOS appear to be more focal than those produced by MNE and those by Whitened ReciPSIICOS. In the activity vs. source index plots this corresponds to sparser (with fewer dots) and narrower populated peaks of activity. In this subject ReciPSIICOS delivers more focal activation than the Whitened ReciPSIICOS approach.

Fig. 15 shows the comparison of reconstructed source timecourses for ReciPSIICOS and LCMV for two subjects, correspondingly. Panel A shows the calculated auditory steady-state responses at 40 Hz. Panel B demonstrates the primary auditory cortex source location which was highly active in both ReciPSIICOS and LCMV solutions. The timecourses of the picked source are shown on Panel C with their envelopes. The blue

line corresponds to ReciPSIICOS, and the orange solid line corresponds to LCMV. As the amplitudes of LCMV activations are by the order of magnitude lower than for ReciPSIICOS, for the visualization purposes, we showed the rescaled LCMV with orange dashed line and highlighted area. What is noticeable here is that for both subjects the ReciPSIICOS reconstruction reveals that the analyzed gamma activity is modulated at a 5-Hz secondary frequency (i.e. theta rhythm), which agrees with the previous study (Doesburg et al., 2012). Panel D shows the distribution of ratio of norms for the LCMV and ReciPSIICOS derived spatial filters. The median value is slightly lower than 1, which confirms that the observed amplitude differences can not be explained by the difference in spatial filter norms. The obtained results are consistent across subjects.

Additionally we have explicitly plotted the SNR maps as a ratio of the post-stim and the pre-stim activation power of the steady-state auditory responses over the hemisphere contralateral to the stimulation where the signal cancellation effect appeared to be most pronounced. As we can see the SNR distribution over the superior temporal cortex and adjacent areas delivered by the proposed methods appears to be several times higher than that observed in the LCMV. The LCMV peaks over the medial cortex. As a gauge we also show MNE solution that reliably discovers contralateral activation.

3.2.2. Dataset 2

The second dataset contains MEG data for the subject that participated in the auditory oddball paradigm and was instructed to press the
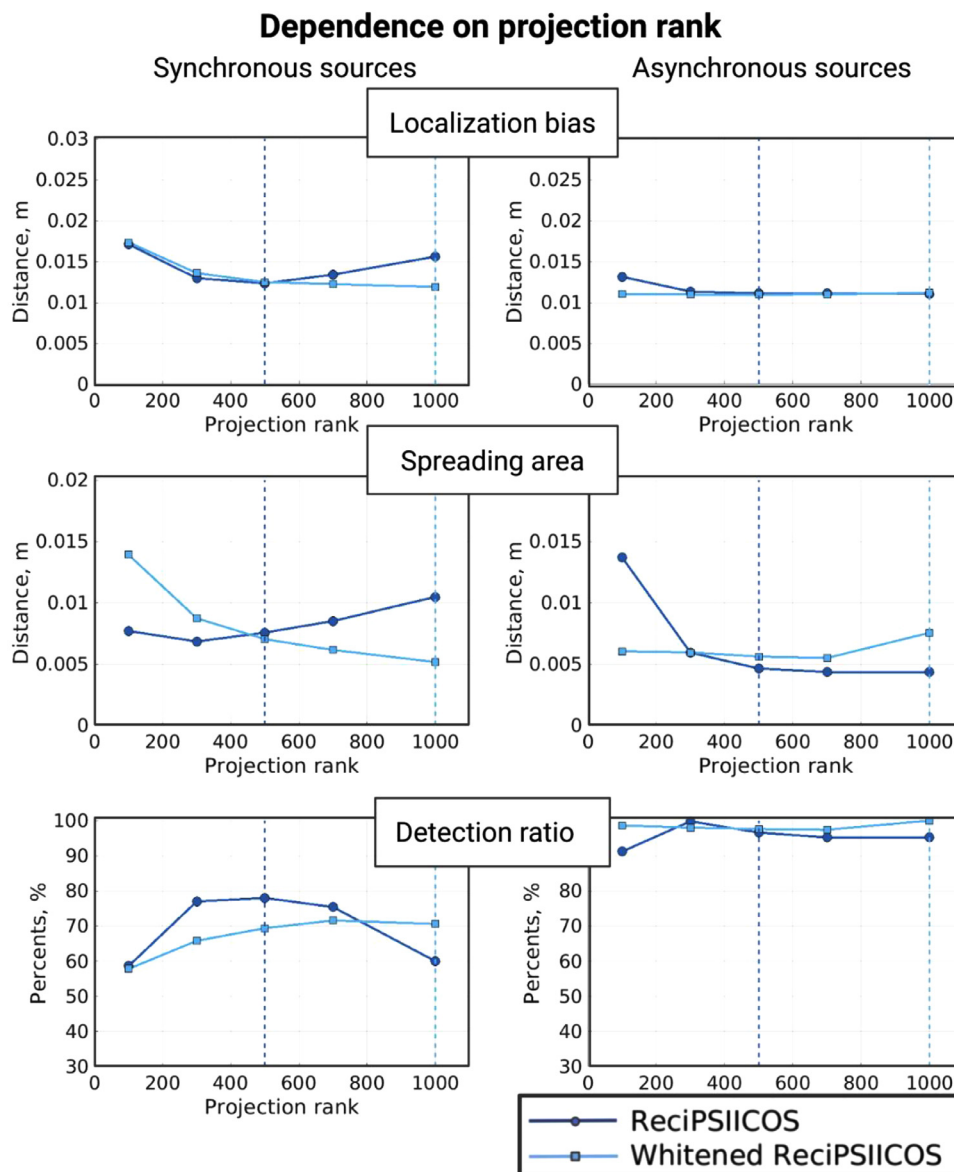
button with the right index finger in response to the deviant stimuli. The stimulation was produced binaurally. Here we are focused on the localization of MMNm component (Näätänen et al., 1994), so after the preprocessing described in Section 2.8.2 we calculated the differential ERF, which is shown on Fig. 17, panel A. The peak of MMNm component is reached at 159 ms post-stimulus, so the inverse problem was solved for this time sample. Panel C shows the activation timeseries for one cortical source (Panel B) highly active both in ReciPSIICOS and LCMV solutions at the target time sample (159 ms post-stimulus). First, as expected, the amplitude reconstructed with LCMV (orange solid line) is significantly lower than the amplitude reconstructed with ReciPSIICOS (blue solid line). In order to compare these two solutions, we rescaled the LCMV solution so that the amplitudes at the target time sample were equal (the area highlighted in orange). It is clearly seen that ReciPSI-ICOS technique allows identifying the source that has one burst significantly different from the background activity. This burst corresponds to the MMNm component. The amplitude of the corresponding peak for LCMV beamformer is comparable with several other distributed along the whole timecourse. To prove that such a difference between the reconstructed amplitudes is due to the signal cancellation effect of the LCMV, but not due to the difference in the spatial filter norms, we cal-

culated for each source the ratio of LCMV coefficients norm to the ReciPSIICOS coefficients norm. The obtained distributions are shown in Panel D. The mean value equals to 0.96 and the standard deviation is 0.14.

Fig. 18 demonstrates the estimated activation maps for ReciPSIICOS, Whitened ReciPSIICOS, LCMV and MNE. While the LCMV beamformer shows the high estimated amplitudes only in primary auditory cortex in the right hemisphere, ReciPSIICOS technique allows to localize activity in both hemispheres. At the same time, Whitened ReciPSIICOS technique shows similar activity in the primary auditory cortices in both hemispheres and an activation in the left motor cortex, which we expected to see due to the motor component of the task. MNE inverse solver found a highly spreaded activation and only in the left hemisphere.

Based on the above, we can state that the experimental data analysis results match those observed for simulated data. The performance of the LCMV beamformer appears to be significantly affected by the presence of correlations between cortical sources while ReciPSIICOS and Whitened ReciPSIICOS remain operable and deliver compact source maps with expected bilateral activation in the primary auditory cortex and a noticeably greater dynamic range.
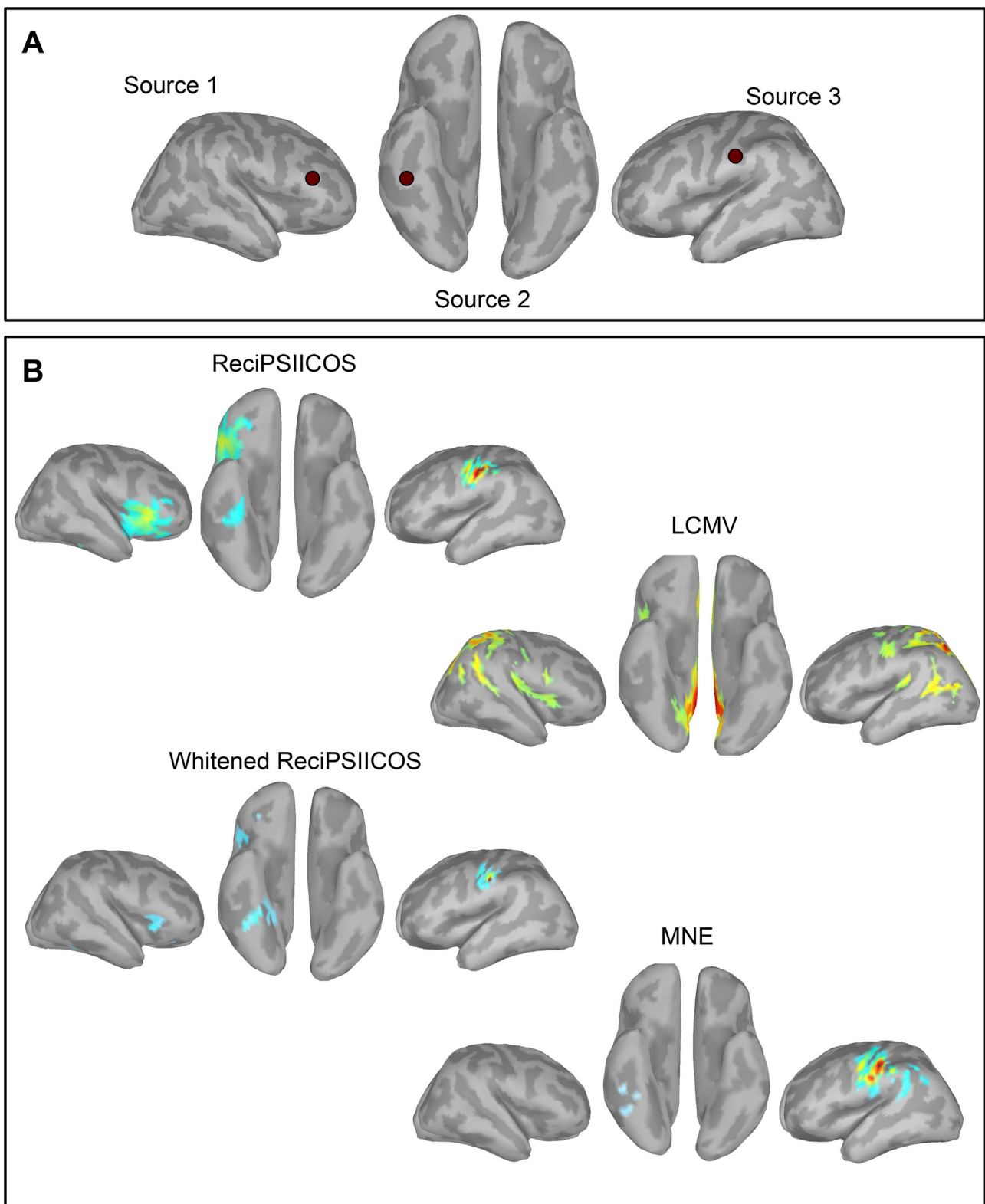
Fig. 10. Modeling the case of three interacting sources. **A**. The locations of three randomly picked sources. **B**. Source activation maps reconstructed with ReciPSIICOS, Whitened ReciPSIICOS, LCMV and MNE.
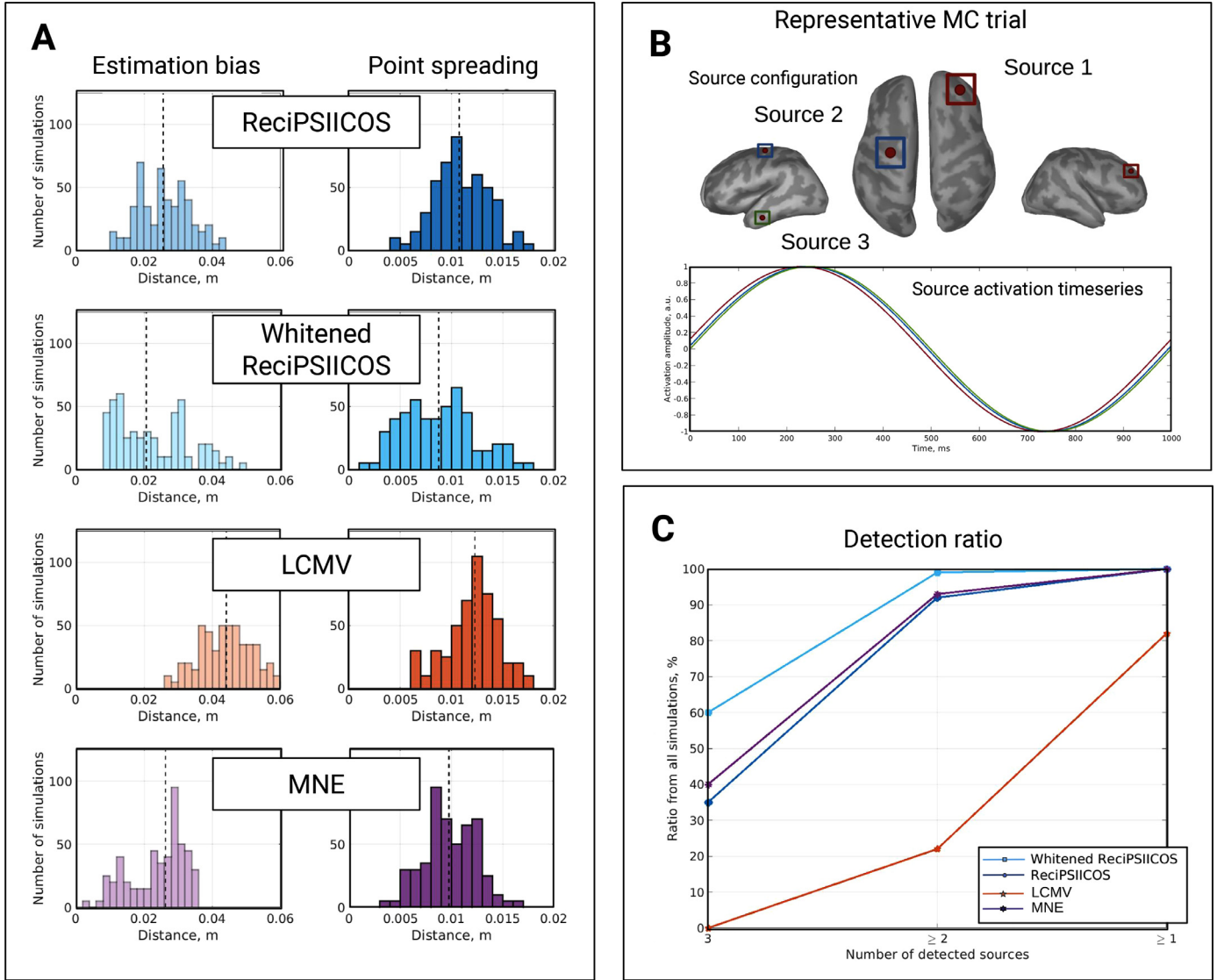
Fig. 11. Simulation of three synchronously active sources. **A.** Distribution of two reconstruction quality metrics: estimation bias and point spreading value, for four reconstruction techniques: ReciPSIICOS, Whitened ReciPSIICOS, LCMV and MNE. **B.** One representative Monte Carlo trial: three cortical sources are randomly picked and activated with the synchronous sinusoidal functions with a random time jitter. **C.** Distribution of the number of detected sources for all simulations.

3.2.3. Non-positive definiteness induced by projection

The proposed approach uses a heuristics expressed in Eq. (19). This step is needed to guarantee that the data covariance matrix modified by the proposed projection remains positive definite (PD). The extent to which this manipulation is justified depends on the amount of "energy" stored in the negative eigenvalues of the reshaped and projected data. We assessed this amount using the expression (24) for the correlation matrices of real MEG datasets.

We estimated the contribution of negative eigenvalues into the total eigenvalue power in terms of L_1-norm:

$$p^- = \frac{\sum_{i=1}^{N_l^-} |\lambda_i^-|}{\sum_{i=1}^{M} |\lambda_i|}, \tag{24}$$

where λ_i, $i = 1 \dots M$ – all eigenvalues of the projected matrix $\widetilde{\mathbf{C}}_x$ and λ_i^-, $i = 1 \dots N_l^-$ are the negative eigenvalues. The contribution of positive eigenvalues in the total power is then $p^+ = 1 - p^-$.

Fig. 19 demonstrates the contribution of positive eigenvalues p^+ as a function of projection rank for ReciPSIICOS and Whitened ReciPSIICOS calculated on Dataset 1 (panel A) and Dataset 2 (panel B). While ReciP-

SIICOS implies the projection on the power subspace, Whitened ReciP-SIICOS performs the projection away from correlation subspace, so in order to align the results, each subplot on Fig. 19 has two x-axes. The lower x-axis corresponds to the ReciPSIICOS and its values are arranged in the descending order. The upper x-axis corresponds to the Whitened ReciPSIICOS and is arranged in the ascending order. Dashed lines show the ranks picked for the analysis. The ratio of positive eigenvalues differs from subject to subject, but in all cases, regardless of the MEG type (CTF or Neuromag), it reaches at least 80% and is typically higher. We therefore suggest the future users of our approach to explicitly monitor the fraction of energy p^- contributed by the negative eigenvalues as defined in (24) and make sure it stays below 20%.

4. Discussion

In agreement with the results of other groups and based on our own analysis, we can state that the adaptive beamformers outperform global methods for solving the inverse problem in cases when the sources can be well described by a small number of focal sources. In this scenario the adaptive beamformers tend on average to deliver more focal source
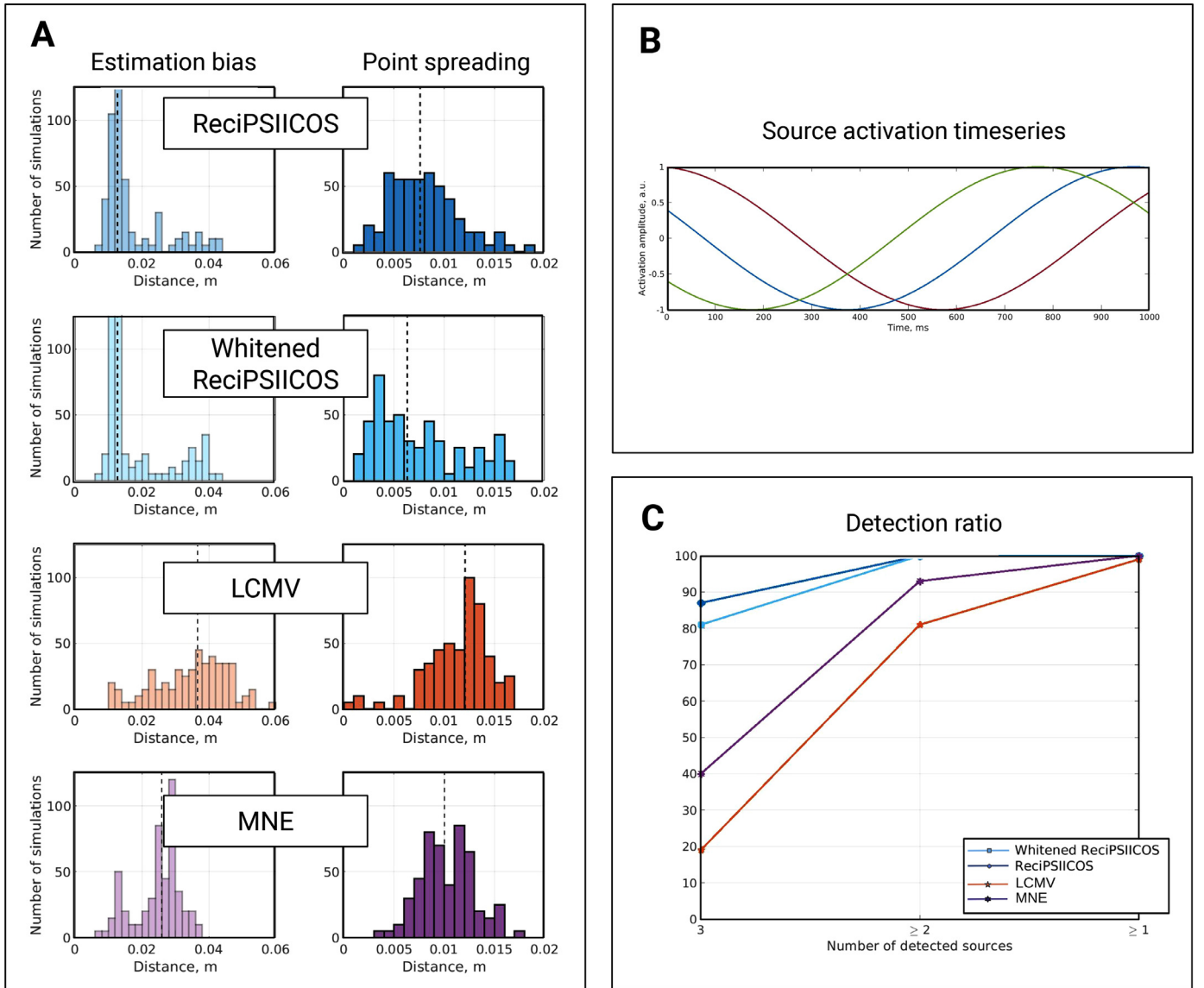
Fig. 12. Simulation of three moderately correlated sources. **A.** Distribution of two reconstruction quality metrics: estimation bias and point spreading value, for four reconstruction techniques: ReciPSIICOS, Whitened ReciPSIICOS, LCMV and MNE. **B.** Example of representative trial: three cortical sources are randomly picked and activated with the sinusoidal functions with relative phase shift of $\frac{\pi}{3}$ and random time jitter. **C.** Distribution of number of detected sources for all simulations.

distribution maps than the methods based on the global optimization. However, the performance of adaptive spatial filters deteriorates significantly in the presence of correlated sources.

In this paper we have developed a novel method to supply robustness to the beamforming technique when operating in the environment with correlated sources. Our approach is based on the consideration of the sensor-space data covariance matrix as an element in a M^2-dimensional space. Using the MEG data generative model, we formulate the generative equation for the data covariance matrix and recognize that it contains contributions modulated by the diagonal elements of the source-space covariance matrix that span S_{pwr}^K subspace as well as its off-diagonal elements that represent coupling of neuronal sources and contributing variance to the coupling subspace S_{cor}^K. Our method then builds a projector away from the subspace modulated by coupling and applies it to the data covariance matrix, effectively removing the contributions brought into the data covariance matrix by the non-orthogonality of the underlying source timeseries.

Strictly speaking, the principal subspaces S_{pwr}^K and S_{cor}^K non-trivially overlap. However, the mutual spatial structure of the auto-terms and

cross-terms allows us to partly disentangle the two subspaces and selectively suppress the variance in one of them while sparing the other.

We have developed two methods for building the projector. The first method simply fills $M^2 \times N$ matrix $\mathbf{G}_{pwr}$ with "topography vectors" as columns and attempts to find the subspace with the smallest dimension that captures maximum variance. This is done via SVD of $\mathbf{G}_{pwr}$ and the first K left singular vectors are then used to build the projector into the subspace they span. This projection is exactly complementary to that described in Ossadtchi et al. (2018) where our goal was to suppress the contribution of volume conduction to the data covariance matrix.

The second approach is somewhat more complex. It projects the observed data correlation away from the S_{cor}^K subspace. To minimize the extent to which such a projection affects the variance in the S_{pwr}^K subspace we perform the projection in the space whitened with respect to the spatial structure of S_{pwr}^K subspace.

Both methods require specifying only a single parameter – rank of the projection K. In Section 2.4, we suggest a natural procedure for the informed choice of K that is based on balancing the rate at which the
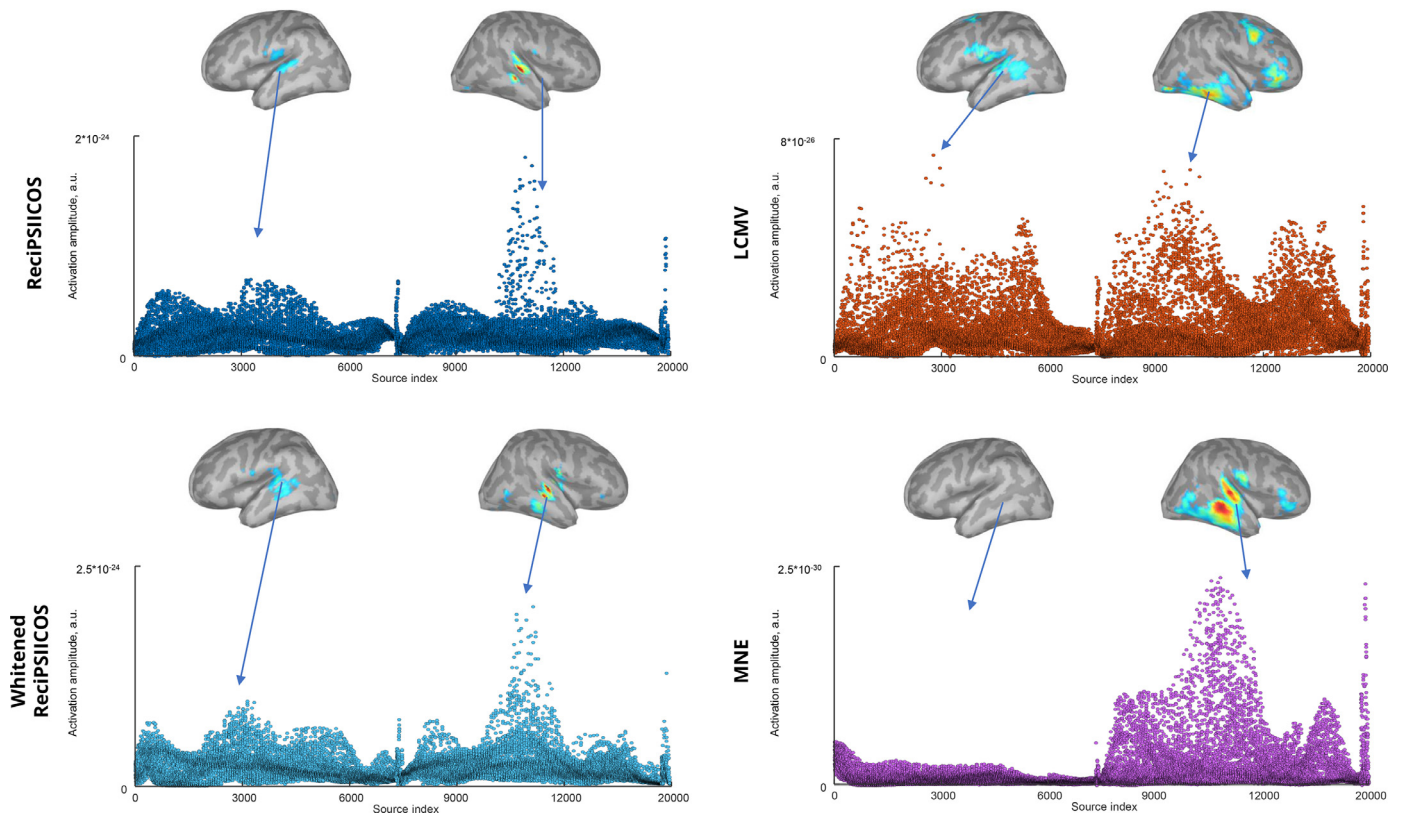
Fig. 13. Power distribution of ASSR at 250 ms post-stimulus reconstructed with ReciPSIICOS, Whitened ReciPSIICOS, LCMV and MNE for the Subject 1.
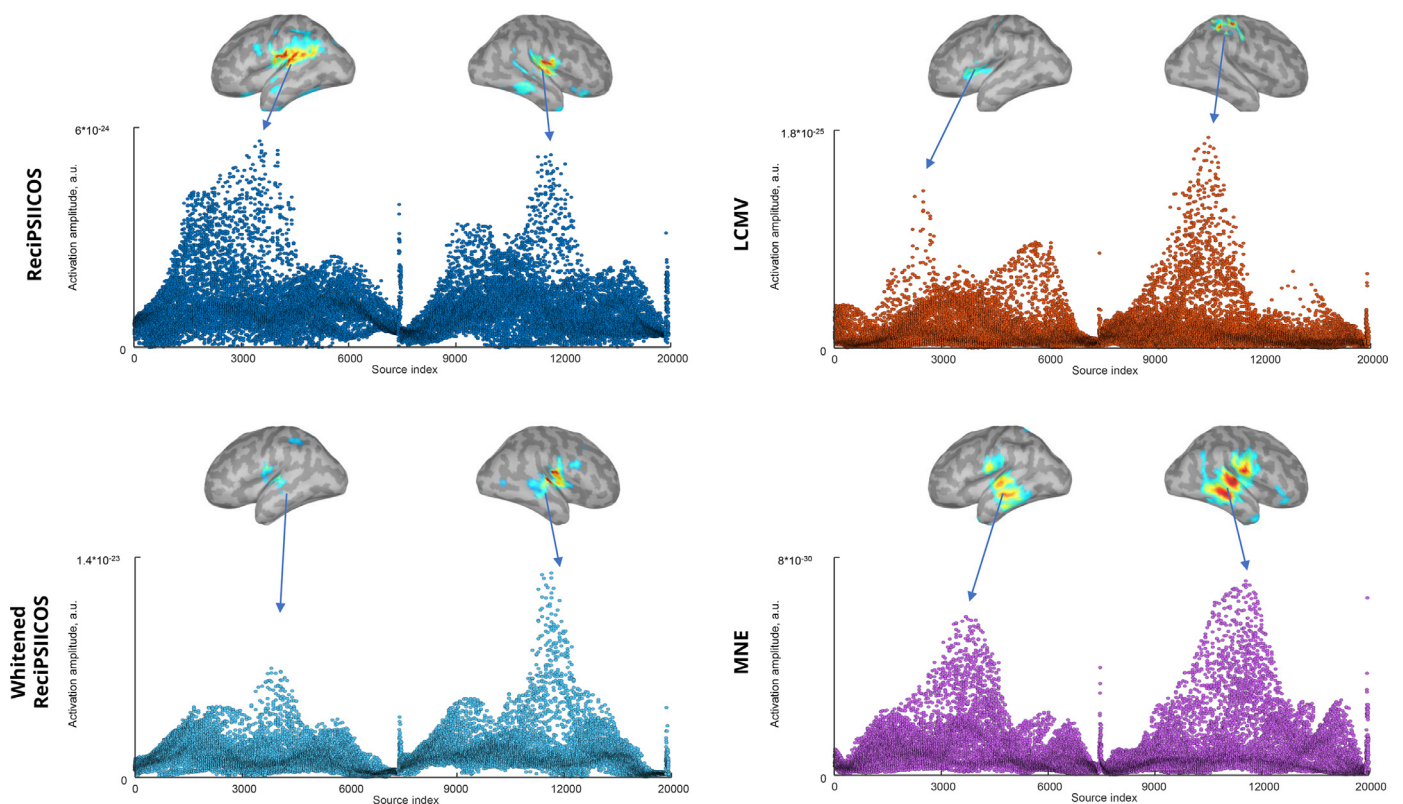

Fig. 14. Power distribution of ASSR at 250 ms post-stimulus reconstructed with ReciPSIICOS, Whitened ReciPSIICOS, LCMV and MNE for the Subject 2.
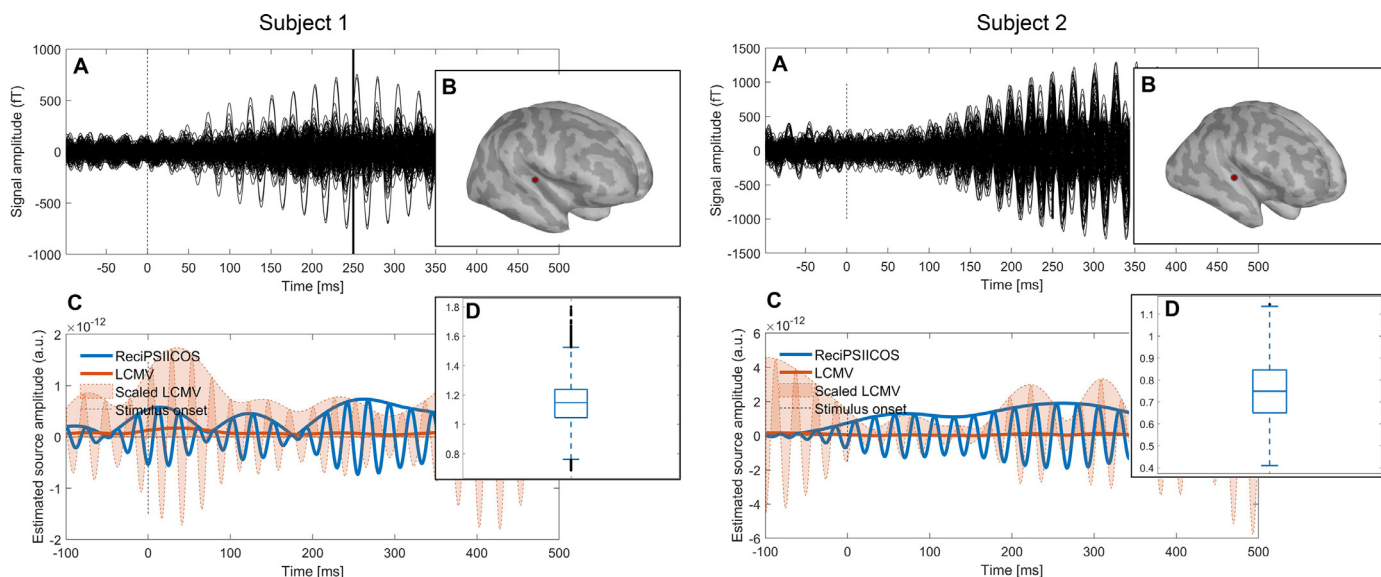
Fig. 15. A. Auditory steady-state responses at 40 Hz. **B**. The cortical source is highly active in both ReciPSIICOS and LCMV solutions at the gamma peak. **C**. The timeseries of a picked source in the primary auditory cortex reconstructed with ReciPSIICOS (solid blue line) and LCMV (solid orange line) techniques. ReciPSIICOS delivers the timeseries amplitude with the magnitudes that is significantly greater than that obtained with the original LCMV. To facilitate a meaningful comparison, an appropriately scaled timeseries estimate with LCMV technique is also shown. **D**. The distribution of ratios of LCMV weight norms to ReciPSIICOS weight norms calculated for each source.
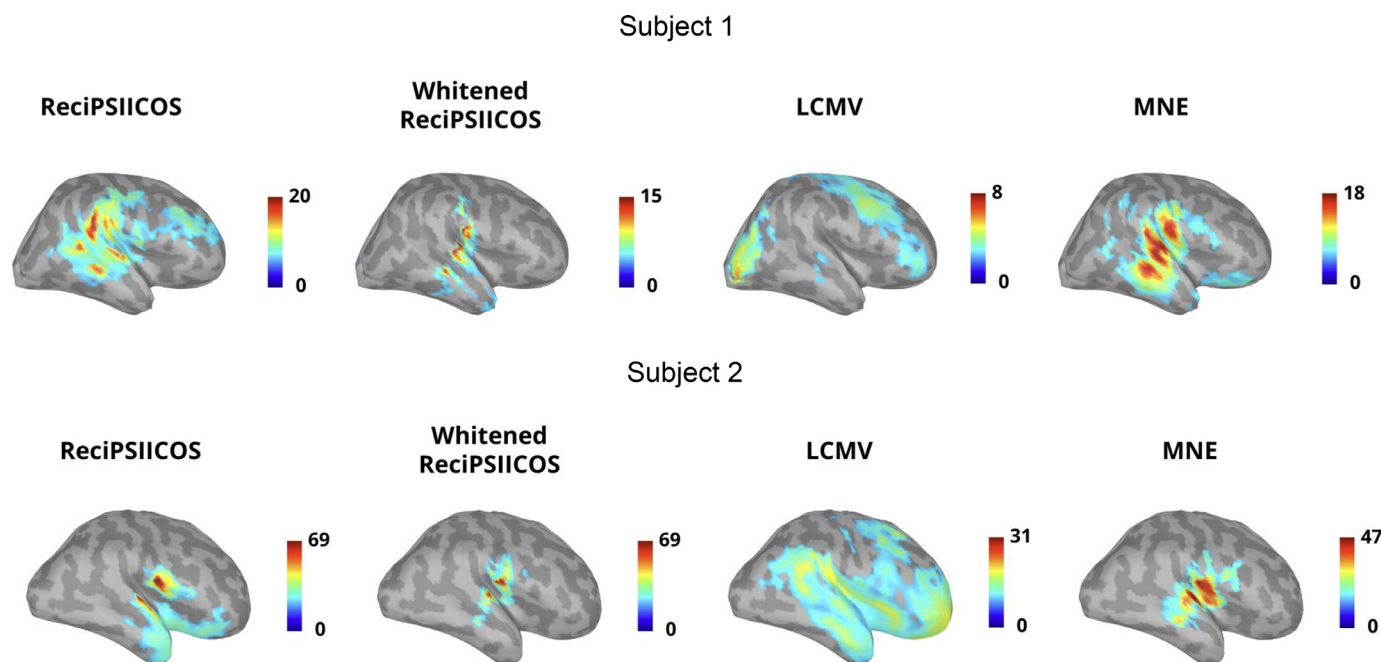

Fig. 16. SNR maps of the auditory steady-state responses computed a ratio of the post-stim and the pre-stim activation for a subject receiving 40 Hz auditory stimulation over the hemisphere contralateral to the stimulation where the signal cancellation effect is most pronounced.

variance is depleted from S_{pwr}^K and S_{cor}^K subspaces with growing projection rank. Overall, we found that the method is quite robust (see Fig. 9) to variations of this parameter in the broad range around the optimal value.

We have also shown that the proposed modification to the original beamforming approach is quite stable and stays functional when operated with realistically accurate forward models. Thus, the proposed technique does not require tuning many parameters and its simplicity is comparable to that of the MNE approach where only regularization parameter λ needs to be adjusted. Our simulations showed that for uncorrelated sources the proposed modification of the covariance matrix

does not adversely affect the performance of the adaptive LCMV beamforming technique. Moreover, in the presence of sources with correlated activity the beamformer built on the basis of ReciPSIICOS projected covariance matrix remains operable and retains adequate localization performance unlike the classical LCMV beamformer. Therefore, the proposed approach can be considered as a modification of the original LCMV technique that relaxes the requirement for source timeseries being uncorrelated.

Additionally, as illustrated in in Fig. 15 (D) the magnitudes of ReciPSIICOS beamformer weight vectors are comparable to those of the LCMV beamformer obtained using the original covariance matrix. Nonethe-
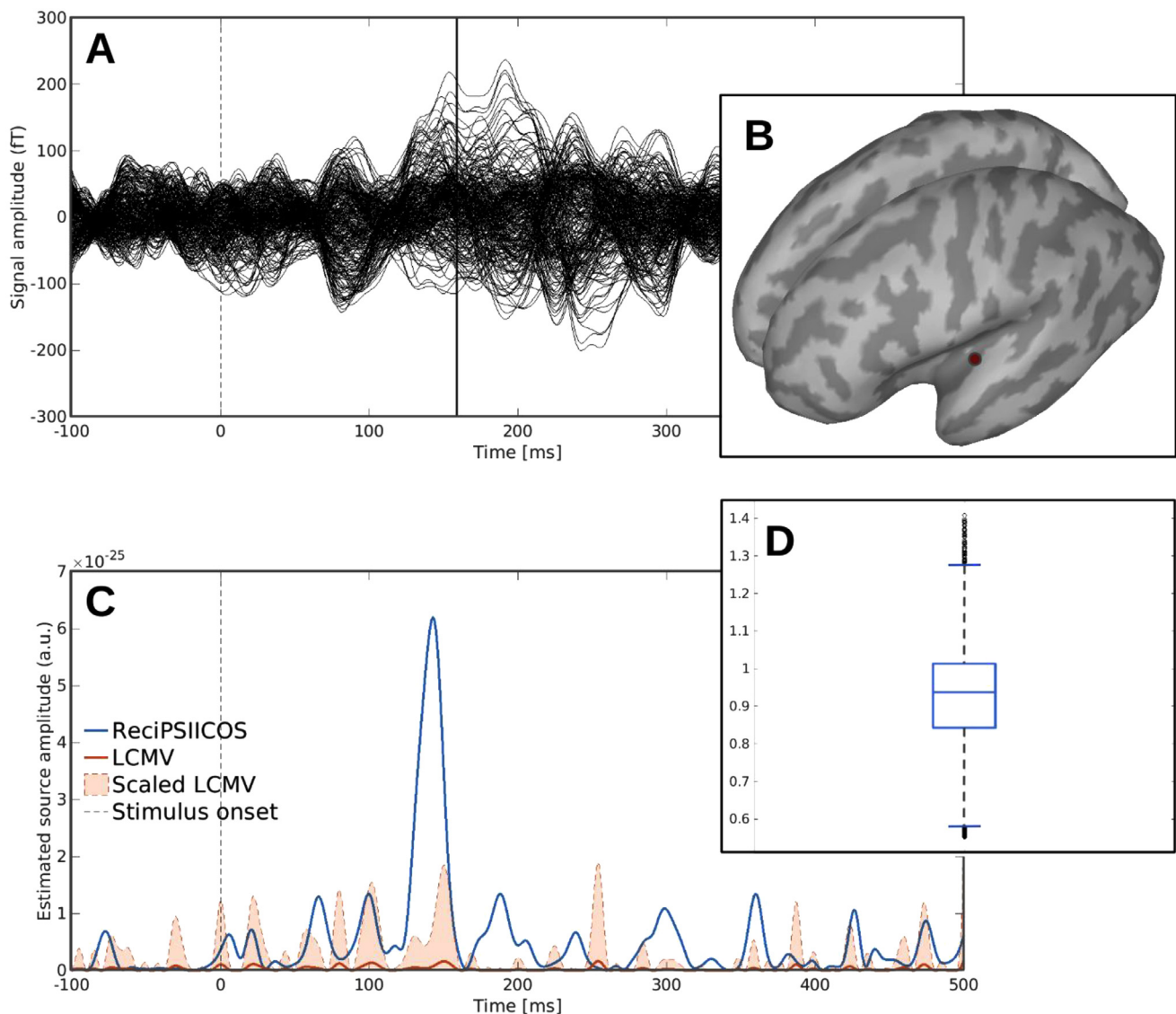
Fig. 17. **A**. The differential ERF timecourses (deviant - standard responses). **B**. The cortical source highly active both in ReciPSIICOS and LCMV solutions at the MMNm peak. **C**. Timeseries of the picked source in the primary auditory cortex reconstructed with ReciPSIICOS (solid blue line) and LCMV (solid orange line) techniques. ReciPSIICOS delivers timeseries amplitude with magnitude significantly greater than that obtained with the original LCMV. To facilitate a meaningful comparison appropriately scaled timeseries estimate with LCMV technique is also shown. **D**. The distribution of ratios of LCMV weight norms to ReciPSIICOS weight norms calculated for each source.

less, the maximum output amplitude of the ReciPSIICOS beamformer exhibits a drastic growth (in some data up to two orders of magnitude!) as compared to the standard LCMV. This property allows for obtaining potentially more informative cortical activation maps of a greater contrast (Figs. 13, 14, 18). We suggest that this result may indirectly gauge the prominence of source-space correlations typically present in the data.

The curves illustrating balance between the suppression of variance in the S_{pwr}^K and S_{cor}^K vary for two different MEG systems. According to the curves in Fig. 5, sensor-array of the Elekta Neuromag system allows for a greater suppression of the undesired variance in the S_{cor}^K subspace practically without affecting that in S_{pwr}^K as compared to the probe of the CTF system. MEG systems based on the optically pumped magnetometers with the sensors located closer to the scalp capture higher spatial frequency harmonics of the magnetic field as compared to the traditional SQUID-based MEG machines. We suggest that the area under the curves shown in Fig. 5 can be used as a design parameter to optimize the sensor layout of the future MEG systems.

As follows from Fig. 16 the timeseries estimated with ReciPSIICOS beamformer are also characterised by a greater SNR than those obtained with MNE or the original LCMV beamformer. Also based on our simulations the difference in the output SNR in the LCMV and modified covariance beamforming approach is observed only in the environments with correlated sources and therefore can be used as a measure of the extent to which correlated sources are present in the data. It is important to realize that there should not necessarily be several well defined sources whose activity is highly correlated. For example it can be the case that several not so strongly correlated sources with the target source will be exploited by the adaptive beamformer weights to minimize the variance at the beamformer output. Our approach drastically reduces chances for this to happen by removing the source synchrony traits from the data covariance matrix. It acts without explicitly finding such correlated sources but bases its operation on the generative model of the sensor-space data covariance matrix.

Based on the simulations and experimental analysis, we conclude that the introduced here ReciPSIICOS and Whitened ReciPSIICOS procedures represent a simple, efficient and data-independent solutions that
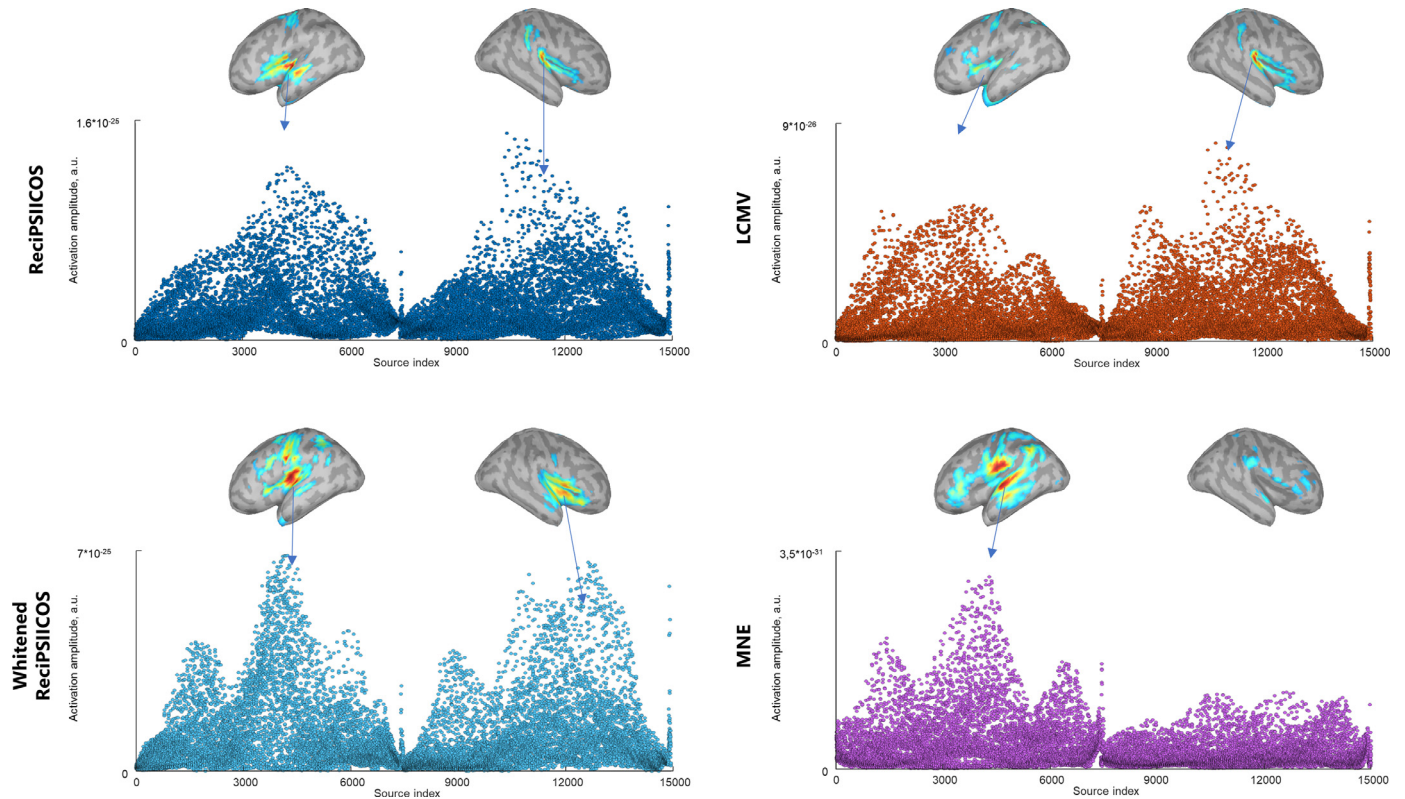
Fig. 18. Reconstructed power distribution with ReciPSIICOS, Whitened ReciPSIICOS, LCMV and MNE for MMNm component at 159 ms post-stimulus.
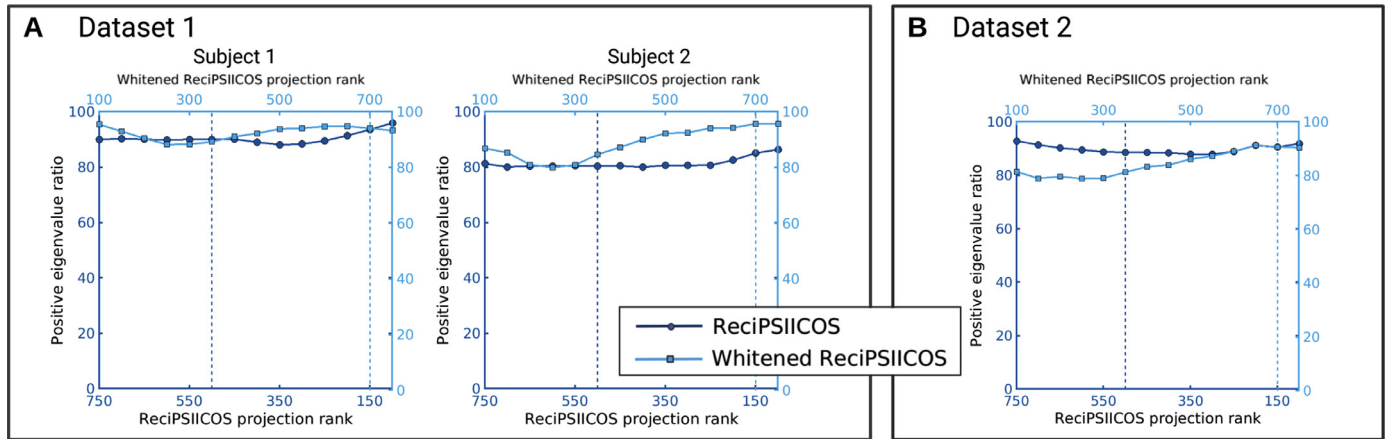

Fig. 19. Contribution of positive eigenvalues of matrix $\widetilde{\mathbf{C}}_x$ in total eigenvalue power as a function of the projection rank for ReciPSIICOS and Whitened ReciPSIICOS for the first MEG dataset (panel **A**) and the second dataset (panel **B**). Dashed lines show the projection ranks picked for the following analysis.

improve the robustness of the adaptive beamforming when operating in the environment with correlated sources. While the original adaptive LCMV beamformer stops operating under these conditions, ReciPSIICOS covariance modification procedure allows to build beamformers that retain spatial resolution properties and maintain high detection ratio when dealing with both synchronous and asynchronous sources.

4.1. Limitations

We did not explicitly study the performance of the proposed approach as a function of the distance between coupled sources. By design of the proposed projection procedure, the components contributed to the data covariance by a pair of correlated proximal sources i and j, more precisely, sources with similar topographies, and sources with dissimi-

lar topographies will be affected differently by both projections. In case of ReciPSIICOS, for proximal sources, the projection into the "power subspace" will not be able to sufficiently weaken the $\mathbf{g}_i\mathbf{g}_j^T + \mathbf{g}_j\mathbf{g}_i^T$ term and the relative contribution to the modified data covariance matrix from synchronous sources with similar topographies will be more pronounced than that from the pair of sources with dissimilar topographies. This will lead to a stronger signal cancellation in cases when a pair of synchronous sources with similar topographies are present in the data. However, the closer the source topographies are, the more difficult it is to cancel these sources because of the limited number of degrees of freedom. In the Whitened ReciPSIICOS case we will observe a similar behavior since the whitening step will attempt to spare from the projection the contribution from the pair of sources with similar topographies. The Whitened ReciPSIICOS approach potentially allows for explicit specifi-

cation of the "refractory zone" around each i-th source when constructing the span of the source-correlation subspace. This may alleviate the undesired behavior when the variance of the close-by highly coupled sources is projected from the data covariance matrix. In both projections this undesired behavior can be hypothetically alleviated if the projectors are built using only active source topographies. This, however, would make the method data-dependent which we wanted to avoid.

Also more computationally expensive, dual- and multi-core beamforming approaches (Diwakar et al., 2011) might be an option here. However, given a large number of factors that may affect the performance of both methods, a separate study is needed to systematically compare the multi-core beamforming approach against the methods proposed here.

The suggested projection procedure does not take into account the Riemannian nature of the manifold of the correlation matrices. Surprisingly, however, the eigenvalue spectrum of the ReciPSIICOS projected matrix remain largely positive. Only a small fraction of eigenvalues are negative and their magnitude is negligible and makes no more than 20% fraction of the total sum of the eigenvalue magnitudes. We return this projection back to the manifold of correlation matrices by simply replacing the negative eigenvalues with their absolute values. Although our results show that this is a reasonable working strategy, the proposed methodology would definitely benefit from the constraints imposed by the configuration of the natural manifold of correlation matrices. Approaches could be adopted in the future similar to the one described in Higham (2002) for finding the element on the manifold of correlation matrices that is the closest to the projected matrix. Overall, until a better solution is adopted to ensure the validity of the obtained imaging results, we recommend exploring the eigenvalue spectrum of the projected matrix and checking that the percentage of the "energy" brought into it by negative eigenvalues does not exceed the 10-20% threshold of the total sum of absolute eigenvalues. We also recommend matching the results against MNE technique that is known for its robustness and although not explicitly designed to image focal sources was shown to manage well when applied to localization of somatosensory sources (Komssi et al., 2004).

In this paper we focused on improving the adaptive beamforming approach that is best applied in the scenario when a few focal sources beget the observed data. Such source configurations are likely to be encountered with ERP/ERF data and represent a set of common assumptions used in the derivation of beamformer for neuroimaging applications starting from the original paper (Van Veen et al., 1997). Our approach does not make any additional assumptions about source distribution and therefore we used the very same model, which was nevertheless shown capable of handling extended sources (De Munck et al., 1988). However, recent findings suggest that the activity underlying even early ERP/ERF components may comprise a complex constellation of sources and therefore novel advanced methods for solving the inverse problem may be needed such as those combining focal and distributed source assumptions (Hauk and Stenroos, 2014). Furthermore, recent phenomenological advances convincingly illustrate that a large proportion of brain activity is present in the form of cortical waves (Alexander et al., 2013) which should motivate the development of novel approaches for source estimation accommodating these novel findings such as Petrov (2012).

5. Funding

References

Ahlfors, S., Han, J., Belliveau, J., Hmlinen, M., 2010. Sensitivity of meg and eeg to source orientation. Brain Topogr. 23, 227–232. doi:10.1007/s10548-010-0154-x.

Alexander, D.M., Jurica, P., Trengove, C., Nikolaev, A.R., Gepshtein, S., Zvyagintsev, M., Mathiak, K., Schulze-Bonhage, A., Ruescher, J., Ball, T., et al., 2013. Traveling waves and trial averaging: the nature of single-trial and averaged brain responses in large-scale cortical signals. Neuroimage 73, 95–112.

An, K.-O., Im, C.-H., Jung, H.-K., 2008. Magnetoencephalography source localization using improved simplex method. Inverse Probl. Sci. Eng. 16 (4), 499–510.

Borgiotti, G., Kaplan, L., 1979. Superresolution of uncorrelated interference sources by using adaptive array techniques. IEEE Trans. Antennas Propag. 27 (6), 842–845. doi:10.1109/tap.1979.1142176.

Brookes, M., Stevenson, C., Barnes, G., Hillebrand, A., Simpson, M., Francis, S., Morris, P., 2007. Beamformer reconstruction of correlated sources using a modified source model. NeuroImage 34, 1454–1465.

Dalal, S., Sekihara, K., Nagarajan, S., 2006. Modified beamformers for coherent source region suppression. IEEE Trans. Biomed. Eng. 53 (7), 1357–1363.

Darvas, F., Pantazis, D., Kucukaltun-Yildirim, E., Leahy, R., 2004. Mapping human brain function with MEG and EEG: methods and validation. NeuroImage 23, S289–S299. doi:10.1016/j.neuroimage.2004.07.014.

De Munck, J.C., Van Dijk, B.W., Spekreijse, H., 1988. Mathematical dipoles are adequate to describe realistic generators of human brain activity. IEEE Trans. Biomed. Eng. 35 (11), 960–966.

Diwakar, M., Huang, M.-X., Srinivasan, R., Harrington, D., Robb, A., Angeles, A., Muzzatti, L., Pakdaman, R., Song, T., Theilmann, R., Lee, R., 2011. Dual-core beamformer for obtaining highly correlated neuronal networks in MEG. NeuroImage 54, 253–263.

Doesburg, S.M., Green, J.J., McDonald, J.J., Ward, L.M., 2012. Theta modulation of interregional gamma synchronization during auditory attention control. Brain Res. 1431, 77–85. doi:10.1016/j.brainres.2011.11.005.

Duin, R.P.W., Pekalska, E., 2010. Non-euclidean dissimilarities: causes and informativeness. In: Hancock, E.R., Wilson, R.C., Windeatt, T., Ulusoy, I., Escolano, F. (Eds.), Structural, Syntactic, and Statistical Pattern Recognition. Springer Berlin Heidelberg, Berlin, Heidelberg, pp. 324–333.

Engemann, D., Gramfort, A., 2014. Automated model selection in covariance estimation and spatial whitening of meg and eeg signals. NeuroImage 108. doi:10.1016/j.neuroimage.2014.12.040.

Fischl, B., 2012. FreeSurfer. NeuroImage 62 (2), 774–781.

Fries, P., 2015. Rhythms for cognition: communication through coherence. Neuron 88 (1), 220–235. doi:10.1016/j.neuron.2015.09.034.

Gascoyne, L., Furlong, P.L., Hillebrand, A., Worthen, S.F., Witton, C., 2016. Localising the auditory n1m with event-related beamformers: localisation accuracy following bilateral and unilateral stimulation. Sci. Rep. 6 (1). doi:10.1038/srep31052.

Greenblatt, R., Ossadtchi, A., Pflieger, M., 2005. Local linear estimators for the bioelectromagnetic inverse problem. IEEE Trans. Biomed. Eng. 53 (9), 3403–3412.

Hamalainen, M., Hari, R., Lmoniemi, R.J., Knuutila, J., Lounasmaa, O.V., 1993. Magnetoencephalography theory, instrumentation and applications to noninvasive studies of the working human brain. Rev. Mod. Phys 65, 413–497.

Hämäläinen, M.S., Ilmoniemi, R.J., 1994. Interpreting magnetic fields of the brain: minimum norm estimates. Med. Biol. Eng. Comput. 32 (1), 35–42. doi:10.1007/bf02512476.

Hauk, O., Stenroos, M., 2014. A framework for the design of flexible cross-talk functions for spatial filtering of meg/eeg data: Deflect. Hum. Brain Mapp. 35 (4), 1642–1653.

Higham, N.J., 2002. Computing the nearest correlation matrix–a problem from finance. IMA J. Numer. Anal. 22 (3), 329–343. doi:10.1093/imanum/22.3.329.

Kimura, T., Kako, M., Kamiyama, H., Ishiyama, A., Kasai, N., Watanabe, Y., 2007. Inverse solution for time-correlated multiple sources using beamformer method. Int. Congress Series 1300, 417–420.

Komssi, S., Huttunen, J., Aronen, H.J., Ilmoniemi, R., 2004. Eeg minimum-norm estimation compared with meg dipole fitting in the localization of somatosensory sources at s1. Clin. Neurophysiol. 115 (3), 534–542.

Luck, S.J., Kappenman, E.S., 2011. The Oxford Handbook of Event-Related Potential Components. Oxford University Press.

Mäkelä, N., Stenroos, M., Sarvas, J., Ilmoniemi, R.J., 2018. Truncated rap-music (trap–music) for meg and eeg source localization. NeuroImage 167, 73–83.

Moiseev, A., Gaspar, J., Schneider, J., Herdman, A., 2011. Application of multi-source minimum variance beamformers for reconstruction of correlated neural activity. NeuroImage 58, 481–496.

Mosher, J., Leahy, R., Lewis, P., 1999. EEG and MEG: forward solutions for inverse methods. IEEE Trans. Biomed. Eng. 46 (3), 245–259. doi:10.1109/10.748978.

Mosher, J.C., Leahy, R.M., 1999. Source localization using recursively applied and projected (rap) music. IEEE Trans. Signal Process. 47 (2), 332–340.

Näätänen, R., Ilmoniemi, R.J., Alho, K., 1994. Magnetoencephalography in studies of human cognitive brain function. Trends Neurosci. 17 (9), 389–395. doi:10.1016/0166-2236(94)90048-5.

Nenonen, J., Nurminen, J., Ki, D., Bikmullina, R., Lioumis, P., Jousmi, V., Taulu, S., Parkkonen, L., Putaala, M., Khknen, S., 2012. Validation of head movement correction and spatiotemporal signal space separation in magnetoencephalography. Clin. Neurophys. 123 (11), 2180–2191. doi:10.1016/j.clinph.2012.03.080.

Ossadtchi, A., Altukhov, D., Jerbi, K., 2018. Phase shift invariant imaging of coherent sources (PSIICOS) from MEG data. NeuroImage 183, 950–971. doi:10.1016/j.neuroimage.2018.08.031.

Petrov, Y., 2012. Harmony: Eeg/meg linear inverse source reconstruction in the anatomical basis of spherical harmonics. PLoS One 7 (10), e44439.

Popescu, M., Popescu, E.-A., Chan, T., Blunt, S., Lewine, J., 2008. Spatio-temporal reconstruction of bilateral auditory steady-state responses using MEG beamformers. IEEE Transactions on biomedical engineering 55 (3), 1092–1102.

Quraan, M.A., Cheyne, D., 2010. Reconstruction of correlated brain activity with adaptive spatial filters in meg. Neuroimage 49 (3), 2387–2400.

Rana, K.D., Hämäläinen, M.S., Vaina, L.M., 2018. Improving the nulling beamformer using subspace suppression. Front. Comput. Neurosci. 12. doi:10.3389/fncom.2018.00035.

Sekihara, K., Nagarajan, S., 2008. Adaptive Spatial Filters for Electromagnetic Brain Imaging. Springer Berlin Heidelberg. doi:10.1007/978-3-540-79370-0.

Sekihara, K., Nagarajan, S., Poeppel, D., Marantz, A., Miyashita, Y., 2001. Reconstructing spatio-temporal activities of neural sources using an MEG vector beamformer technique. IEEE Trans. Biomed. Eng. 48 (7), 760–771. doi:10.1109/10.930901.

Tadel, F., Baillet, S., Mosher, J., Pantazis, D., Leahy, R., 2011. Brainstorm: a user-friendly application for MEG/EEG analysis. Comput. Intell. Neurosci. doi:10.1155/2011/879716.

Taulu, S., Simola, J., 2006. Spatiotemporal signal space separation method for rejecting nearby interference in meg measurements. Phys. Med. Biol. 51, 1759–1768. doi:10.1088/0031-9155/51/7/008.

Van Veen, B., Van Drongelen, W., Yuchtman, M., Suzuki, A., 1997. Localization of brain electrical activity via linearly constrained minimum variance spatial filtering. IEEE Trans. Biomed. Eng. 44 (9), 867–880. doi:10.1109/10.623056.

Varela, F., Lachaux, J.-P., Rodriguez, E., Martinerie, J., 2001. The brainweb: Phase synchronization and large-scale integration. Nat. Rev. Neurosci. 2 (4), 229–239. doi:10.1038/35067550.